

Investigating the role of intestinal stromal cells in inflammation and infection

By

Jessica Pei

Department of Microbiology and Immunology

McGill University, Montreal, Quebec, Canada

July 2022

A thesis submitted to McGill University in partial fulfillment of the requirements of the degree
of Master of Science

© Jessica Pei, 2022

TABLE OF CONTENTS

Abstract.....	5
Résumé.....	5
Acknowledgements.....	7
Contribution of Authors.....	8
Abbreviations.....	9
CHAPTER 1: INTRODUCTION AND LITERATURE REVIEW.....	12
1.1 Overview of the mammalian gastrointestinal tract.....	12
1.2 Cellular architecture of the crypt-villus and crypt axis.....	12
1.3 The intestinal epithelium.....	15
1.3.1 LGR5+ intestinal stem cells.....	15
1.3.2 Reserve and damage-associated intestinal stem cell populations.....	16
1.3.3 Absorptive Lineages.....	17
1.3.4 Secretory lineages.....	17
1.4 Stem cell niche: stromal-epithelial crosstalk.....	21
1.4.1 Wnt and R-spondin signaling pathways.....	21
1.4.2 BMP signaling pathway.....	23
1.4.3 Hedgehog signaling pathway.....	24
1.4.4 Notch signaling pathway.....	26
1.5 Stromal cells.....	28
1.5.1 Fibroblasts.....	29
1.5.2 Myofibroblasts.....	29
1.5.3 Telocytes.....	30
1.5.4 Trophocytes.....	31
1.6 Disruption of homeostasis during intestinal inflammation and infection.....	33

1.6.1 Inflammatory Bowel Disease	33
1.6.2 Enteropathogenic and enterohemorrhagic <i>Escherichia coli</i>	35
1.6.3 <i>Citrobacter rodentium</i>	36
CHAPTER 2: MATERIALS AND METHODS	38
2.1 Experimental animals.....	38
2.2 Gut Preparation	38
2.3 scRNAseq.....	38
2.4 <i>C. rodentium</i> infection.....	39
2.5 Lineage tracing experiments in irradiated intestine of mice	40
2.6 DSS treatment	40
2.7 Primary stromal cell cultures	40
2.8 Immunohistochemistry and immunofluorescence	41
2.9 Fluorescent <i>in situ</i> hybridization.....	42
2.10 Organoid culture.....	43
2.11 Quantitative real-time qPCR.....	44
CHAPTER 3: RESULTS.....	45
3.1 Aim 1. Analyze the response of the intestinal stromal cell compartment following infection with <i>C. rodentium</i>	45
3.1.1 scRNAseq analysis of the intestinal stromal compartment at d6 and 13 post <i>C. rodentium</i> infection.....	45
3.1.2 <i>Cd109⁺Ifi44⁺</i> IAFs are localized at the tops of colonic crypts and appear transiently at early timepoints of infection.....	47
3.1.3 Treatment of primary stromal fibroblasts with IFN- γ and heat killed <i>C. rodentium</i> results in an upregulation of interferon stimulated genes and IAF markers.....	51
3.1.4 Assessing the <i>in vivo</i> role of <i>Cd109⁺</i> IAFs in models of intestinal inflammation and infection.	52

3.2 Aim 2. Determine the ability of stromal cell secreted factors to mediate intestinal epithelial phenotype in inflammation and regeneration.....	53
3.2.1 Using a stromal-derived conditioned media model to understand stromal-epithelial signal mediation.....	53
3.2.2 Stromal-derived PGE2 may induce a fetal reprogramming response in the intestinal epithelium	55
3.2.3 Investigating the role of PGE2 on intestinal epithelial wound healing <i>in vivo</i>	57
CHAPTER 4: DISCUSSION.....	60
4.1 Aim 1 – Analyzing the response of the intestinal stromal cell compartment following infection with <i>C. rodentium</i>	60
4.2 Aim 2.1 – Modeling stromal-epithelial signaling in an <i>ex vivo</i> setting.....	63
4.3 Aim 2.2 – Modeling the effect of stromal-derived PGE2 on intestinal epithelial regeneration <i>in vivo</i>	65
CHAPTER 5: CONCLUSION	67
References.....	68

Abstract

The maintenance of intestinal homeostasis is an intricately regulated process comprised of several dynamic components, including a self-renewing epithelium and a heterogeneous stromal cell compartment in the underlying lamina propria. Stromal cells were previously overlooked as passive structural cells. However, a growing body of evidence indicates that they play active roles in maintaining homeostasis by regulating the intestinal stem cell niche and the epithelial barrier. Conversely, the role of intestinal stromal cell subsets in the intestinal response to inflammation and infection is less well characterized. We hypothesized that under infectious and inflammatory conditions, stromal cells contribute to intestinal remodeling and drive regenerative signaling of the epithelium. To elucidate the response of the stroma to infectious conditions, *Citrobacter rodentium* was employed as an intestinal infection model. Through single-cell RNA sequencing, we have demonstrated that upon infection, the stromal cell compartment undergoes a remodeling event. Specifically, at early timepoints post infection, a novel and transient *Cd109⁺Ifi44⁺* inflammatory-associated fibroblast (IAF) population appears. *In situ* hybridization studies revealed that these IAFs are localized at the top of colonic crypts. Additionally, to investigate the role of IAFs in intestinal inflammation and infection *in vivo*, we subjected *Cd109* WT and KO mice to dextran sulfate sodium-mediated colitis and *C. rodentium* infection. To understand how stromal cells mediate intestinal epithelial stem cell renewal, we have also developed *ex vivo* conditioned media organoid assays. Our results using this system suggest that stromal cells secrete prostaglandin-E2, a soluble lipid, that interacts with epithelial cells and promotes intestinal epithelial remodeling. Overall, these studies will contribute to a greater understanding of the role of stromal cells in responding to infectious agents and inflammatory damage of the intestinal tract.

Résumé

Le maintien de l'homéostasie intestinale est un processus régulé de manière complexe, composé de plusieurs éléments dynamiques, dont un épithélium qui se renouvelle automatiquement et un compartiment sous-jacent de cellules stromales hétérogènes. Les cellules stromales étaient auparavant considérées comme des cellules structurelles passives. Cependant, un nombre croissant de résultats indique qu'elles jouent un rôle actif dans le maintien de l'homéostasie en régulant la niche des cellules souches intestinales et la barrière épithéliale. À l'inverse, le rôle des cellules stromales intestinales dans la réponse intestinale à l'inflammation et à l'infection est

moins bien caractérisé. Nous postulons que suite à une infection ou en présence de signaux inflammatoires, les cellules stromales contribuent au remodelage intestinal et dirigent la signalisation régénérative de l'épithélium. Pour élucider la réponse du stroma face à un agent infectieux, *Citrobacter rodentium* a été utilisé comme modèle murin d'infection intestinale. Grâce au séquençage de l'ARN sur cellule unique, nous avons démontré que lors de l'infection, le compartiment cellulaire du stroma subit un remodelage. Plus précisément, à des moments précoces après l'infection, nous avons remarqué l'apparition d'une nouvelle population transitoire de fibroblastes inflammatoires (FIs) marqués par l'expression des gènes *Cd109* et *Ifi44*. Des études d'hybridation *in situ* ont révélé que ces FIs sont localisés au sommet des cryptes du colôn. En outre, pour étudier le rôle des FIs dans l'inflammation et l'infection intestinales *in vivo*, nous avons soumis des souris *Cd109* WT et KO à une colite provoquée par le dextran sulfate de sodium et à une infection par *C. rodentium*. Pour comprendre comment les cellules stromales médient le renouvellement des cellules souches épithéliales intestinales, nous avons également développé des essais organoïdes en milieu conditionné *ex vivo*. Les résultats obtenus avec ce système suggèrent que les cellules stromales sécrètent de la prostaglandine-E2, un lipide soluble, qui interagit avec les cellules épithéliales et favorise le remodelage épithélial intestinal. Globalement, ces études permettront de mieux comprendre le rôle des cellules stromales dans la réponse aux agents infectieux et aux lésions inflammatoires du tractus intestinal.

Acknowledgements

Reflecting on these past two years of graduate school, I cannot help but feel grateful for every mentor, friend, and peer that has contributed to my graduate student experience thus far.

First, I would like to thank my wonderful supervisors Dr. Samantha Gruenheid and Dr. Alex Gregorieff for their mentorship throughout my undergraduate and master's degree. You have taught me the fundamentals of how to approach scientific questions and challenges. I am extremely grateful for your patience, support, and encouragement throughout my early scientific career. You have both created an extremely positive environment to learn, make mistakes, and grow as a trainee but also an individual. Thank you for trusting me and believing in me.

I would also like to thank my advisory committee Dr. Irah King and Dr. Nathalie Perrault for their mentorship. Your input was extremely valuable and helped shape my project to where it is today.

Additionally, I would like to thank my wonderful lab mates, past and present, who have helped me significantly throughout my degrees and during covid. To both the Gruenheid and Gregorieff lab members – thank you for your mentorship and above all your friendship throughout these past years. Thank you to Dr. Brendan Cordeiro for being an incredible mentor to me during my undergraduate project, I truly don't think I'd be where I am without your guidance, patience, and consistent encouragement. You've pushed me to be a better student and taught me to be independent. Also thank you to Lindsay, Tyler, and Brendan for being amazing trivia partners, twisted tea buddies, and all-around labbies. I thoroughly enjoyed our time in the lab together, and you're right, the Bellini Death Grip is indeed real. Likewise thank you to the other incredible Gruenie's Goonies – Alex, Christina, Hicham, and Lei for your continued support and guidance in the lab, you are each incredibly knowledgeable and I will have so much to learn. Also, your shared love for Donato the First and Donato Jr. has been a source of entertainment and happiness for me. Thank you to Wimmy and Morgan for your energy and support during this writing process, I am excited to see all the incredible things the next generation of Goonies will do! To the members of the Gregorieff lab – Julia, Tanvi, Annie, Majd, and Aaron, thank you for all the laughs, amazing conversations in the STC, and for your constant support – it means a lot, and it is with a heavy heart that I am saying goodbye. Additionally, I would like to thank Sherilyn and Adam from the

Stratton laboratory for all their help and knowledge of scRNAseq and contributions to this project. It's always nice to have your bright and cheerful energy in the lab!

I am also extremely grateful for my roommate June, who was always one door away for a chat, a laugh, or a cry. I could not have done these last two years without you, your company throughout the pandemic has kept me sane, and you are truly a ray of sunshine and a shoulder to lean on. Also shout out to all my wonderful friends in Montreal who have helped me throughout my undergrad and masters: Rebecca, Jeehyun, Selin, Montana, Priya, Lucia, Jason, Jayson, David, Jon, Hanshi, and Liam, you have always all brought smiles to my face, and I've enjoyed every moment we've spent together. Additionally, thank you to my amazing friends from home: Caroline, Laura, Haley, Matt, and Yichen who have encouraged me and supported me for so many years. A special shout out to Minoli as well for all the time we've spent writing together, your encouragement these past ten years means so much to me.

I would also like to thank my wonderful and supportive family, my sister Marina, and my parents Xiaomei and Jian. Your words of encouragement have gotten me through this process, and I would not be where I am without your love and support.

Lastly, I would like to dedicate this thesis to my late Uncle Ergang, one of the most passionate scientists I had the pleasure to know. Thank you for your incredible excitement for science and for inspiring me to continue being curious. Your contributions and your impact will not be forgotten. I hope to continue making you proud, you will be forever missed.

Contribution of Authors

All the described chapters were written and performed by me as primary author under direct supervision of Dr. Samantha Gruenheid and Dr. Alex Gregorieff.

Gut preparations of *Citrobacter rodentium* infected mice were completed by the efforts of Dr. Brendan Cordeiro and Sherilyn Recinto. scRNAseq and data analysis was completed by the collaborative efforts of Sherilyn Recinto and Adam MacDonald.

Abbreviations

A/E – Attaching and Effacing

APC – Adenomatous polyposis coli

α SMA – Alpha smooth muscle actin

BMP – Bone morphogenic protein

BMPi – Bone morphogenic protein inhibitor

CAF – Cancer-associated fibroblast

CLU – Clusterin

CM – Conditioned media

DASC – Damage-associated stem cell

Dhh – Desert Hedgehog

DSC – Deep secretory cell

DSS – Dextran sodium sulfate

ECM – Extracellular Matrix

EEC – Enteroendocrine cells

EHEC – Enterohemorrhagic *E. coli*

EPEC – Enteropathogenic *E. coli*

FACS – Fluorescence-activated Cell Sorting

FFPE – Formalin-fixed paraffin-embedded

FISH – Fluorescent *in situ* hybridization

Fz – Frizzled

GALT – Gut associated lymphoid tissue

GI – Gastrointestinal

Gli1/2/3 – Glioblastoma 1, 2, 3

GPI – Glycosylphosphatidylinositol

GSK3 – Glycogen synthase kinase

Hh – Hedgehog

IAF – Inflammatory-associated fibroblasts

IBD – Inflammatory Bowel Disease

IF- Immunofluorescence

IFN – Interferon

IgA – Immunoglobulin A

IHC – Immunohistochemistry

Ihh – Indian Hedgehog

IL – Interlukin

ILC2 – Type II innate lymphoid cells

ilCAF – Interferon-licensed Cancer-associated fibroblasts

IND – Indomethacin

ISC – Intestinal stem cells

ISG – Interferon stimulated genes

LEE – Locus of Enterocyte Effacement

LGR5 – Leucine-rich repeat-containing G-protein coupled receptor 5

M cell – Microfold cell

MUC – Mucins

myCAF – myofibroblast Cancer-associated fibroblast

NICD – Notch intracellular domain

PDGFR α – Platelet-Derived Growth Factor Receptor alpha

PGE2 – Prostaglandin E2

PGH2 – Prostaglandin H2

Ptch – Patched

qPCR – Quantitative Polymerase chain reaction

rISC – Reserve intestinal stem cells

RSPO – R-spondin

scRNAseq – Single cell RNA sequencing

Shh – Sonic Hedgehog

SI – Small intestine

Smo – Smoothed

Stx – Shiga Toxin

T3SS – Type III secretion system

TA – Transit Amplifying cell

TAM – Tamoxifen

TGF – Transforming growth factor

TGF- β – Tumour growth factor β

Tir – Translocated Intimin Receptor

TNF – Tumor necrosis factor

UC – Ulcerative colitis

UMI – Unique molecular identifier

WAE – Wound-associated epithelium

YAP – Yes-Associated Protein

CHAPTER 1: INTRODUCTION AND LITERATURE REVIEW

1.1 Overview of the mammalian gastrointestinal tract

The mammalian gastrointestinal (GI) tract is a multi-organ system comprised of the mouth, esophagus, stomach, small intestine (SI), colon, and rectum (1). Together, they are primarily responsible for the coordination of food digestion and absorption of nutrients to be distributed throughout the body (1). However, in addition to digestion and absorption, the GI tract is endlessly multitasking through self-renewal of the intestinal epithelium, immune surveillance, and maintaining tolerance to the microbiota (2). Given these roles, several components help maintain the intricate regulation of intestinal homeostasis. These players include a self-renewing epithelium, communities of stromal and immune cells interlaced in underlying lamina propria, and gradients of secreted factors mediating crosstalk between these cells (3).

Upon ingestion, food travels to the stomach and becomes partially digested by gastric acid and enzymes – producing a semifluid mass of food called chyme (1, 4). The chyme is then mobilized to the SI – divided into the duodenum, jejunum, and ileum (1). The SI is where the majority of nutrient, water, and electrolyte absorption occurs. Here, chyme is further broken down into subunits of proteins, fats, carbohydrates, and vitamins which are absorbed by intestinal epithelial cells to be distributed throughout the body (5). The remaining undigested material is then pushed into the colon. Secondary to the SI, the colon is also a key player in nutrient digestion and absorption (6). Here, complex carbohydrates and proteins previously resistant to digestion are broken down by resident commensal bacteria which aid in fermentation of undigested materials. In addition, the water from the remaining material is reabsorbed, which becomes compacted into stool prepared for expulsion via the rectum (1, 4).

1.2 Cellular architecture of the crypt-villus and crypt axis

The cellular architecture of the SI and colon are quite distinct, ultimately reflecting their respective functional requirements (7). Owing to the role of the SI in digestion and nutrient absorption, its epithelium is organized into millions of crypt-villus units to increase the digestive and absorptive surface (2, 7). A villus is a finger like protrusion projecting into the intestinal lumen, covered in an epithelial monolayer of post-mitotic cells (7). A dense network of capillaries and

lymph vessels protrude into the villi beneath the epithelium to absorb nutrients and distribute them to the liver, and subsequently the rest of the body (7). The base of each villus is also surrounded by several epithelial invaginations into the intestinal wall, called crypts of Lieberkühn (7, 8) (**Figure 1**). These crypts harbour populations of adult intestinal stem cells (ISCs) that proliferate and fuel the self-renewal of the epithelium (8). Notably, specialized cells in the crypt promote the continuous outflow of mucus and anti-microbial products to flush any contaminants out and protect the resident ISCs (9). As form follows function, the colon specializes in compacting and mobilizing stool for excretion. Therefore, in contrast to the SI, the colon does not contain any villi, instead it is characterized by a flat luminal surface containing only crypt invaginations (2).

The wall of the SI and colon are also organized in four concentric layers comprised of the mucosa, submucosa, muscularis propria, and serosa (5) (**Figure 2**). Beginning with the inner most layer, the mucosa is further subdivided into the epithelium, lamina propria, and muscularis mucosa (1). The intestinal epithelium provides a physical barrier between the luminal contents and the rest of the host tissue (2). Lying underneath the epithelium is the lamina propria – a layer of connective tissue that hosts a broad population of stromal cells, as well as infiltrating immune cells (1). The third component of the mucosa is the muscularis mucosa – a thin layer of smooth muscle cells (1). Following is the submucosa which provides structural support to the mucosa and is resident to blood and lymphatic vessels. Here, the submucosa also harbours the Meissner plexus encompassing a network of nerves that make up components of the enteric nervous system (ENS) (5, 10). Specifically, neuronal bodies of the Meissner plexus innervate the intestinal crypts and villi, aiding with the regulation of absorptive and secretory activity (10). Next, the muscularis propria is made up of a circular and longitudinal layer of smooth muscle tissue that sandwiches the myenteric plexus, another component making up the ENS (11). Here, the neuronal cell bodies originate in the myenteric plexus, and innervate the circular and longitudinal smooth muscle layers, responsible for initiation and control of smooth muscle motor patterns (10). Finally, the outer most layer is the serosa, which connects the gut wall to the mesentery (1).

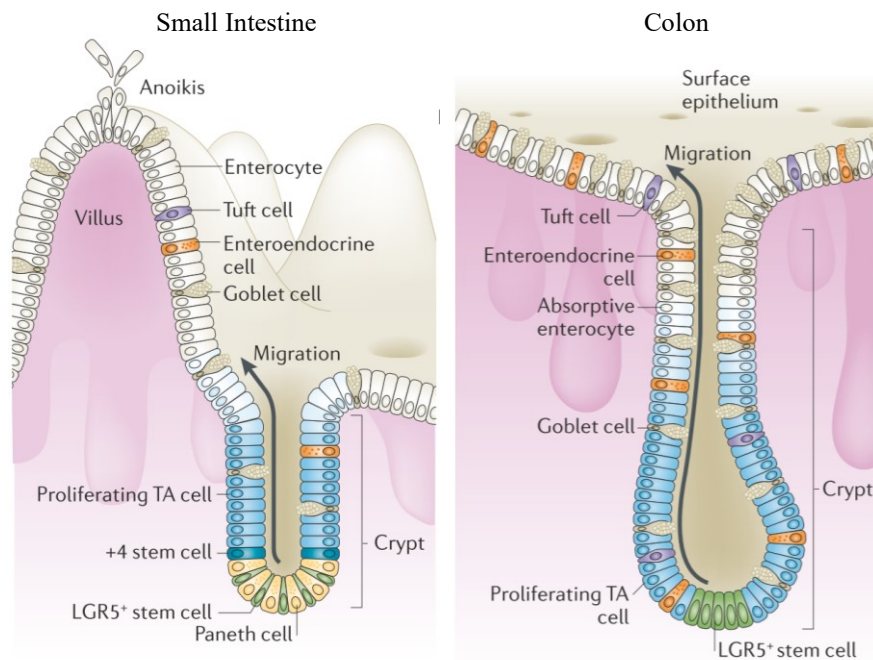


Figure 1. Cell migration and lineage specification up the crypt-villus axis and crypt axis of the small intestine and colon, respectively. The intestinal epithelium rapidly renews every 3-5 days. $Lgr5^+$ ISC at the base of intestinal crypts will drive this regeneration through proliferation in the stem cell niche followed by differentiation. When undergoing differentiation, cells will migrate up the crypt-villus axis of the SI or the crypt axis of the colon to become transit amplifying cells acting as progenitors that eventually take on one of six epithelial cell lineages (Enterocyte, Tuft cell, Enteroendocrine cell, goblet cell, Paneth cell, or M cell (not depicted)). Paneth cells exist exceptionally in the SI and will migrate downwards upon differentiation from the TA zone back to the intestinal stem cell niche. Adapted from (2).

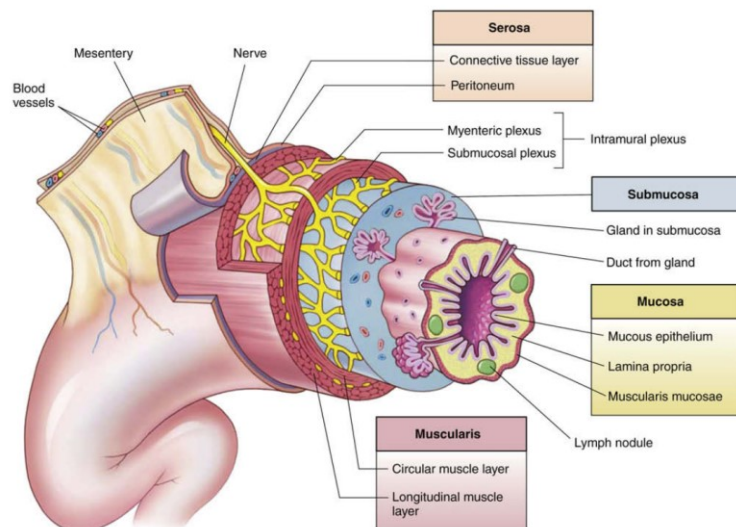


Figure 2. The four concentric layers of the intestinal wall: Mucosa, Submucosa, Muscularis Mucosa, and Serosa. From the inner most layer, the mucosa is comprised of the epithelium, the lamina propria, and muscularis mucosae. Following is the submucosa in which blood and lymphatic vessels are located, as well as the Meisner Plexus, a component of the ENS system. Next is the muscularis propria comprised of the circular and smooth muscle layers followed by the serosa, the outer most layer, connecting the gut wall to the mesentery. Adapted from (1).

1.3 The intestinal epithelium

The epithelium of the GI tract is one of the most rapidly self-renewing systems in mammals, regenerating every 3-5 days (12). It must achieve efficient digestion and absorption of food contents, while maintaining an effective physical barrier from commensal microbiota, dietary antigens, toxins, and pathogens (2). To accomplish these tasks, the epithelial monolayer contains six specialized cell lineages with distinct roles. Notably, these lineages are all derived from the same pool of $Lgr5^+$ ISC residing at the base of the intestinal crypt (**Figure 3**). Their differentiation is prompted by cues from the surrounding stem cell niche, in which ISCs will proliferate then differentiate up the crypt-villus or crypt axis (2). Eventually they are shed in the lumen at the villus tip or crypt apex (9).

1.3.1 LGR5+ intestinal stem cells

Homeostatic renewal of epithelial cells is mediated by ISCs residing at the base of crypts (12). While ISCs, also termed crypt-base columnar cells (CBCs), were first identified and morphologically characterized using electron microscopy in 1974, their further validation as an adult stem cell population was made possible through genetic lineage tracing experiments performed only several decades after (13). In 2007, a prominent Wnt-pathway controlled gene – Leucine-rich repeat-containing G-protein coupled receptor 5 (*Lgr5*) was identified as a specific marker for ISCs (14). Indeed, an *in vivo* lineage tracing through a *Lgr5* specific, heritable *LacZ* reporter gene, demonstrated that *lacZ*⁺ cells resided at the crypt base (14). Additionally, after several days *lacZ*⁺ progeny were observed in cells extending from the crypt base to the villus tips of the small intestine, and similarly observed in the colon. These *lacZ*⁺ cells were present in all cell lineages and persisted throughout the life span of the mouse (14). Thus demonstrating that $Lgr5^+$ ISCs fit the two major requirements of an adult stem cell, (1) being multipotent by giving rise to all cell types in the resident tissue and (2) having long-term self renewal abilities (14).

$Lgr5^+$ ISCs must both maintain the stem cell pool but also give rise to progenitors that go on to make up the six epithelial cell lineages broadly categorized as absorptive and secretory epithelial cells (15). The dynamics of self-renewal are as follows. $Lgr5^+$ ISCs proliferate at the base giving rise to transit-amplifying (TA) progenitor cells (16). These TA cells will divide 4-5 times before being pushed out of the crypt base (stem cell zone), migrating further up the crypt axis and receiving signals that induce terminal differentiation into absorptive (enterocytes,

Microfold cells (M cells) or secretory (Paneth, goblet, enteroendocrine, tuft cell) lineages (16, 17). Nearing the end of their life cycle, epithelial cells are pushed from the villus tips into the lumen through the process of anoikis, with the exception of Paneth cells that migrate downwards towards the crypt upon differentiation. From here the gaps left by shedding epithelial cells are continuously replaced through generation of new cells from Lgr5⁺ ISCs (15).

1.3.2 Reserve and damage-associated intestinal stem cell populations

In addition to actively cycling Lgr5⁺ ISCs driving homeostatic renewal of the epithelium, investigators have also proposed a secondary stem cell pool called reserve intestinal stem cells (rISCs) (17). While rISCs do not normally perform stem cell function, they are suggested to be slow-cycling, radio-resistant, and have the capacity to reconstitute the Lgr5⁺ ISC population after severe damage or physiological stress (17). For instance, during radiation treatment which results in the complete loss of Lgr5⁺ ISCs (17–20). Historically, these rISC populations are referred to as +4 reserve stem cells (owing to their location 4 cell spaces from the crypt base), and identified through markers such as *Hopx*, *Bmi1*, *Tert*, and *Lrig1* (21–24). Indeed, several studies have demonstrated that complete ablation of Lgr5⁺ ISCs through diphtheria toxin-induced cell death or irradiation results in little impact on the homeostatic renewal of the epithelium, as it is still able to recover and reconstitute itself (15, 20). This suggests that rISCs resistant to damage could compensate and replenish the pool of lost Lgr5⁺ ISCs (19).

However, in recent years, the term +4 rISCs has become restrictive and outdated, as other regenerative stem cells in other crypt locations have been determined. For instance, Clusterin⁺ (Clu⁺) revival stem cells (RevSCs) have been identified using single-cell transcriptomics (25). These Clu⁺ cells are proposed to be multipotent, capable of giving rise to all epithelial cell lineages including Lgr5⁺ ISCs; however, they are extremely rare under homeostasis (25). Instead, Clu⁺ cells undergo a transient expansion and regenerate the damaged epithelium during severe injury induced by irradiation, dextran sodium sulfate (DSS) treatment, or ablation of Lgr5⁺ ISCs (25). It should be noted that it is still unknown how Clu⁺ cells are related to other cell populations that contain inducible stem cell potential (25, 26).

The term +4 rISC has also become controversial in recent years, as contradictory lines of thought propose that differentiated or partially differentiated progenitor cells are responsible for dedifferentiating and repopulating the Lgr5⁺ ISCs during severe epithelial damage (15). Studies

have shown that epithelial lineage progenitors, such as DLL1⁺ secretory progenitors and enterocyte progenitors can both replenish the ISC pool and contribute to the intestinal lineages (27, 28). Likewise, it has been noted that many markers enriched in the +4 position rISCs indeed overlap with progenitor populations (27, 28).

For the purpose of this thesis, these damage-associated rISCs and RevSCs will be referred to together as damage-associated stem cells (DASC)s.

1.3.3 Absorptive Lineages

Enterocytes are derived from absorptive progenitors, and can account for up to 80% of total intestinal epithelial cells (29, 30). Morphologically, they are highly polarized and contain apical brush-border microvilli that protrude into the lumen. The brush border is essential for their enterocyte function, aiding in uptake of ions, water, nutrients, vitamins, and unconjugated bile salts across the epithelium (31). In addition to their absorptive roles, enterocytes also assume active roles in maintaining a physical barrier between the lumen and host tissue, as well as immunological functions (32). Notably, enterocytes produce antimicrobial peptides to target bacteria as well as cytokines to coordinate immune responses. They also coordinate the transportation of immunoglobulin A (IgA) from the basolateral surface into the lumen, which plays a prominent role in maintaining homeostasis and tolerance between the host tissue and the microbiota (33).

Microfold cells (M cells) are specialized absorptive cells lining the gut-lymphoid tissues (GALTs) of the intestine, specifically in Peyer's patches of the SI, caecal patches, or colonic patches (34, 35). With the apical side of the cell facing the lumen, they capture immunogenic particles and transport them across the mucosal barrier to deliver to dendritic cells and other immune cells of the submucosa (35). M cells can be morphologically distinguished from other epithelial cells through two dominant features: the lack of microvilli and the presence of a basolateral pocket (35). Often B cells are found within the basolateral pocket and have been shown to inhabit it for the entirety of the M cells life span, for unknown reasons (35).

1.3.4 Secretory lineages

Goblet cells are a secretory lineage whose major function is mucus production. They will form a gel-like protective barrier of mucus over the epithelial surface to provide a first line of defense against luminal threats (32). Goblet cells can be morphologically identified through their resemblance to a drinking goblet, owing to the fact that their cellular cytoplasm is filled with

secretory granules containing mucins (MUCs) near the apical surface (36). MUCs are highly glycosylated proteins that provide the major building blocks of mucus; specifically, MUC2 is the dominant mucin produced by goblet cells and makes up the majority of the mucus layer in the colon (37). There are two types of mucus organizations in the GI tract: the colon is comprised of two mucus layers, an inner and an outer, whereas the SI only contains a single layer (37). Notably, the singular mucus layer in the SI is very loose and unattached, similar to the outer layer of the colon (38). In contrast, the colon's inner layer of mucus is "firmly" attached to the epithelial cells and is normally less penetrable to bacteria under homeostatic conditions (38). This layer is continuously renewed by secretion from goblet cells, whereby secretion of MUC2 interacts with the previously secreted layer, forming large net-like structures (37, 38).

In addition to mucin production, goblet cells also secrete other factors that contribute to intestinal barrier maintenance and immune protection. For instance, they secrete resistin-like molecule β which modifies T cell mediated immunity and trefoil factor 3 (TFF3) which promotes epithelial restitution after mucosal injury (39). They can also acquire soluble antigens from the intestinal lumen and deliver them to dendritic cells (32).

Enteroendocrine cells (EECs) are secretory cells that release hormone peptides, regulating digestion and motility of the gut (40). Although they make up less than 1% of the total epithelial lineages, EECs represent the largest endocrine organ in the body (40, 41). Notably, EECs comprise 12 known subtypes that arise from a common enteroendocrine progenitor (42). Historically, these subtypes were identified based on a "one-cell one hormone" notion where one subtype was presumed to only produce one hormone (42). For instance, M cells were named based on their secretion of motilin, whereas L cells were named based on their containment of large vesicles (42). Now with scRNAseq, a greater understanding of EEC diversity shows overlap between secreted hormones (42). To date there are 20 known EEC-derived peptide hormones that mediate gut function, with variable expression patterns along the GI tract (42). In the colon, EECs produce serotonin, glucagon-like peptide, insulin-like peptide, and neurotensin (42).

Paneth cells are a secretory lineage unique to the epithelium of the SI. They are located at the base of intestinal crypts, interspersed between Lgr5⁺ ISCs (32). Paneth cells are abundant secretors of antimicrobial peptides and proteins like defensins, C-type lectins, lysozymes, and phospholipases, playing important roles in host-defense and mediation of innate immunity (32,

43). These factors will protect against infections from enteric pathogens, as well as shape the composition of the commensal microbiota (43). Given their abundant secretory role, hallmarks of Paneth cell ultrastructure resemble that of professional secretory cells, including an extensive endoplasmic reticulum and Golgi network with apical clustering of secretory granules (43, 44). Paneth cells also differ from all other specialized epithelial cell lineages, during differentiation they migrate downwards and settle in the crypt, rather than up the crypt-villus axis (44). The lifespan of the Paneth cell is also quite long-lived, persisting for up to a month compared to other lineages that live only 3-5 days (44). In addition to antimicrobial production, Paneth cells also play a vital role in SI epithelial renewal and ISC regulation. Due to their positioning adjacent to ISCs, they secrete many factors that help maintain the proliferative capacity and stemness of ISCs. Paneth cells secrete EGF, Wnt3, and Notch ligand Dll4, all core components of ISC maintenance (7, 32, 45).

Deep crypt secretory (DCS) cells are a population of secretory cells unique to the colon and fulfill functions similar to Paneth cells of the SI. They are marked by Reg4⁺ and located within the ISC niche, intermingled between Lgr5⁺ ISCs. Like Paneth cells, they contribute to the maintenance of Lgr5⁺ ISCs by secreting EGF and expressing Notch ligands (46). Ablation of DCS cells through diphtheria-toxin (DT) injection in Reg4^{DTR} mice results in progressive loss of stem cells from the colonic crypts. However, Lgr5⁺ ISCs were able to recover upon arrest of DT administration (46). It should also be noted that unlike Paneth cells, DSC cells do not produce Wnt3, but there is evidence that stromal cells surrounding the crypt provide a source of Wnts, contributing to colonic ISC maintenance (Reviewed in section 1.5) (46, 47).

Tuft cells are a rare chemosensory epithelial lineage making up 0.4% to 2% of the intestinal epithelium (48). Characteristically, their microvilli are gathered in “tuft” like structures, extending apically into the lumen (49). The role of tuft cells remained unclear until recent years, where three independent reports identified them as prominent players in type II immunity, specifically against parasitic helminth and protozoa infections (50–52). Tuft cells are the sole source of IL-25, a cytokine essential in the response to parasites as this signal recruits and promotes the expansion of type II innate lymphoid cells (ILC2s) (50–52). ILC2s then secrete IL-13, a prominent cytokine in the “weep and sweep” response to parasitic infection. Notably, IL-13 secretion will also act on epithelial progenitors to promote lineage specification of tuft and goblet cells, resulting in a positive feedback circuit between tuft cell and ILC2 signaling (48, 49, 53). Therefore, disruption of tuft cell formation leads to impaired type II immune response and delayed parasite expulsion.

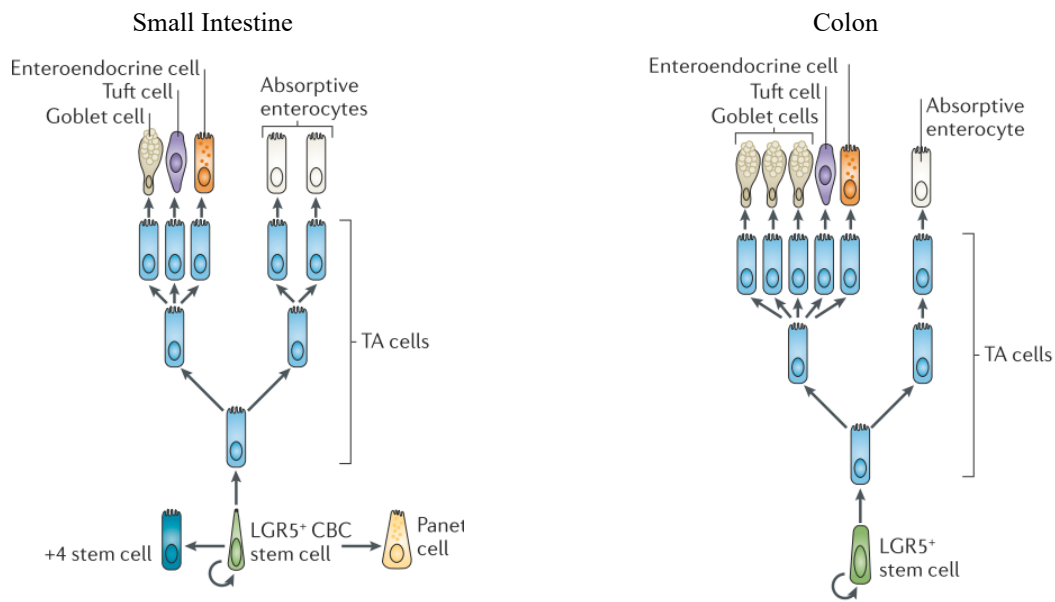


Figure 3. Hierarchy of epithelial cell lineage differentiation within the small intestine and colon. Beginning with the Lgr5⁺ ISCs, they will differentiate into transit amplifying cells comprised of absorptive and secretory progenitors. Following they will differentiate into one of six epithelial lineages (SI: Enterocytes, Tuft cell, Goblet cell, Paneth cell, Enteroendocrine cell, M cell (not depicted), Colon: Enterocyte, Tuft cell, Goblet cell, Enteroendocrine cell, Deep secretory cell (not depicted) and M cell (not depicted)). Adapted from (2).

1.4 Stem cell niche: stromal-epithelial crosstalk

The stem cell niche and subepithelial microenvironment are essential regulators of intestinal epithelial regeneration. Given the coordination of proliferation and differentiation events within the crypt compartment, strict signaling gradients are required to dictate epithelial fate (11). These signaling gradients are provided by subsets of stromal cells that form a dense network underneath the intestinal epithelial monolayer. They will communicate bi-directionally through soluble mediators to maintain the ISC niche and differentiated epithelial lineages under homeostatic conditions (11). Together, stromal cell subsets and epithelial cells engage in a crosstalk through three major signaling pathways: Wnt, Bone morphogenic protein (BMP), and Hedgehog (Hh), as well as cell-cell signaling through Notch pathways to regulate ISC proliferation and differentiation (26, 47).

1.4.1 Wnt and R-spondin signaling pathways

The Wnt signaling pathway is evolutionarily conserved across many biological processes, ranging from embryonic development to homeostatic maintenance of adult tissue (54). In the context of the intestine, Wnt signaling is a major regulator of Lgr5⁺ ISC proliferation and stem cell maintenance (45, 55). Wnt concentration therefore follows a gradient along the crypt-villus or crypt axis in which the signal is highest at the base of the crypt, and slowly decreases up the axis (56). In the small intestine, this gradient is maintained through Wnt secretion of Paneth cells interspersed between ISCs, as well as stromal cells directly adjacent to stem cells located at the base of the crypt (56). However, in the colon, Wnt signaling is primarily secreted by surrounding stromal cells (discussed further in section 1.5) (56).

In the canonical pathway, Wnt signaling relies on β -catenin as a primary signal transducer to activate downstream signaling events (54). Under steady state, when no Wnt signaling is present, β -catenin signaling is inactive due to its degradation by a “destruction complex” composed of Axin, Adenomatous polyposis coli (APC), and glycogen synthase kinase (Gsk3). Together, this complex facilitates β -catenin ubiquitination, targeting it for proteasomal degradation (**Figure 4A**) (54). However, under active Wnt signaling, Wnt binds to the Frizzled (Fz) receptor, initiating a cascade that inactivates the destruction complex (**Figure 4B**). This allows for stabilization and accumulation of β -catenin in the cytoplasm, and eventual translocation in the nucleus (54). Once translocated, β -catenin will co-operate with the transcription factor, TCF4, forming the TCF4/ β -

catenin complex, where together they promote the transcription of genes essential for ISC proliferation, including additional Wnts (55, 57). Canonical Wnt signaling has undoubtedly the most important influence on maintaining the undifferentiated state of ISCs. For instance, knocking out the main effector of the Wnt pathway, TCF4, leads to complete loss of ISCs (58). Likewise, epithelial specific deletion of β -catenin results in the loss of the intestinal epithelium within six days of ablation (59). Conversely, constitutive activation of β -catenin in ISCs or mutation of the APC destruction complex induces hyperproliferation of the intestinal epithelium (60). Taken together, these studies demonstrate the critical role Wnts play in maintaining ISC function and controlling homeostatic levels of stem cell proliferation.

In addition to Wnts, the signaling pathway also requires agonists known as R-spondins (RSPO). The signal strength of Wnts relies on the ability for the Fz receptor to accumulate at the cell surface (57). However, activity of membrane bound ubiquitin ligases RNF43 and ZNF3 mediate ubiquitination, internalization, and degradation of the Fz receptor. RSPOs mediate a secondary ligand-receptor interaction with LGR receptors, binding together with RNF43/ZNF3, preventing Fz from being degraded (57). Thus, RSPO is referred to as a potentiator of Wnt signaling by allowing it to bind to Fz and maintain a prolonged signal transduction (57).

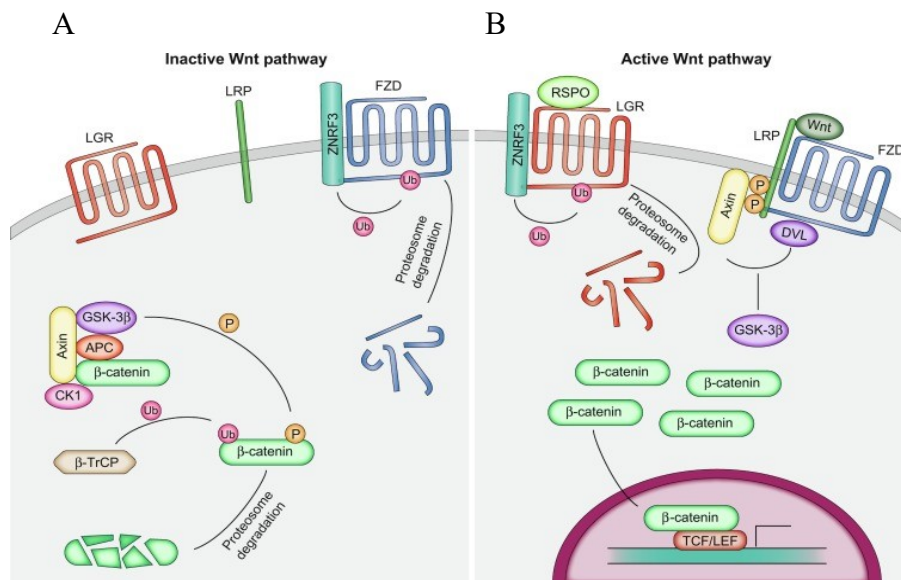


Figure 4. Inactive and active canonical Wnt signaling cascade. (A) When Wnt is not present, β -catenin becomes phosphorylated by the “destruction complex” made up of Axin, APC, and Gsk3. β -catenin is therefore targeted for ubiquitination and proteasomal degradation. (B) When Wnt is present, it binds to the Frizzled (Fz) receptor initiating the inactivation of the destruction complex. Following, β -catenin accumulates within the cytoplasm and translocates to the nucleus where it will bind to the TCF4 transcriptional factor, promoting transcription of Wnt target genes. When RSPO is present, it will bind to the LGR receptor and sequester RNF43/ZNF3 preventing Fz receptor degradation, potentiating Wnt signaling. Adapted from (57).

1.4.2 BMP signaling pathway

Contrary to Wnts, BMP signaling is responsible for inhibiting ISC expansion, and instead, promoting lineage specification of progenitors into terminally differentiated epithelial cells. The gradient of BMP signaling is opposite to Wnts: that is, the signal is most concentrated at the top of villi or apex of crypts and decreases towards the crypt base (47). The BMP gradient is maintained through high secretion of BMP ligands from stromal cells surrounding the villi or crypt apex, with other stromal populations secreting BMP inhibitors (BMPis) at the crypt base (61). Major BMPis include Grem1, Grem2, Chordin-like 1, and Noggin (61).

BMPs are signaling proteins belonging to the tumour growth factor (TGF)- β superfamily. They signal through serine/threonine kinase receptor subtypes I and II (BMPRI and BMPRII, respectively) (62). Upon BMP binding, in the canonical signaling pathway, BMPRI becomes phosphorylated by BMPRII which results in downstream phosphorylation of several intracellular signaling transducers, SMAD 1, 5, and 8 (pSMAD1/5/8). This results in the formation of a complex with SMAD4, and together they enter the nucleus to induce transcription of BMP target genes (62) (**Figure 5**).

The roles of BMP signaling are two-fold: they are required for (1) controlling the levels of ISC proliferation and (2) the maturation of certain epithelial lineages. It has been well described that BMP restricts intestinal epithelial hyperproliferation. In humans, germ line mutations in BMP type I receptor, BMPRIA, or the SMAD4 signal transducer can result in juvenile polyposis syndrome, causing the formation of ectopic epithelial invaginations and increased risk of colorectal cancer (63). These phenotypes are recapitulated in mice with overexpression of BMP inhibitor, Noggin, or deletion of BMPRI1A, resulting in formation of ectopic crypts along with expansion of Lgr5⁺ stem cell pools. This suggests that BMP signaling restricts stemness of Lgr5⁺ ISCs (63, 64). However, in addition to hyperproliferation, inhibition of BMP signaling also results in impaired differentiation of the secretory lineages like goblet cells, Paneth cells, and EECs (65). In an epithelial specific knockout of the receptor BMPRI (Villin-Cre; *Bmpr1a*^{fl/fl}), there is dysregulated

goblet cell maturation, reduced terminal differentiation of Paneth cells, and a 75% reduction in EECs per crypt-villus units (65). This suggests that BMPs facilitate lineage commitment in certain secretory cells (65).

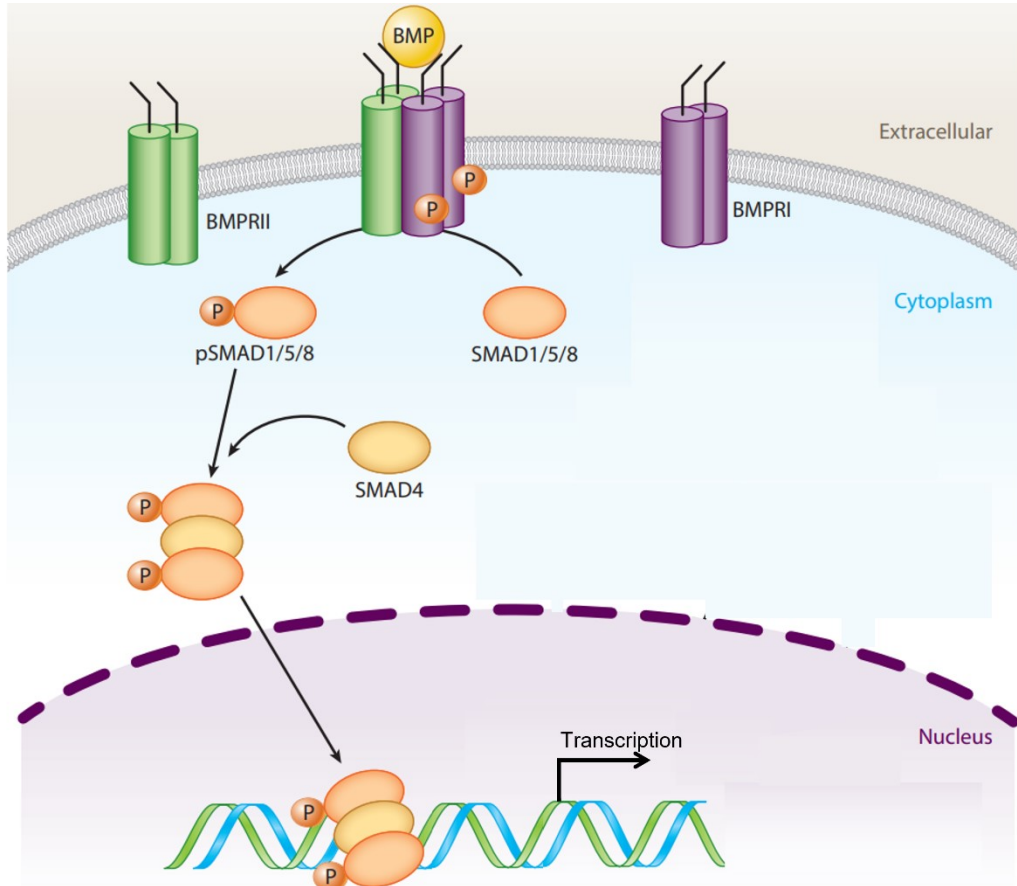


Figure 5. Canonical bone morphogenic protein (BMP) signaling pathway. When BMP ligands are present, they will bind to a type II receptor (BMPRII) which will bind and phosphorylate a type I receptor (BMPRI). Upon these binding and phosphorylation events, BMPRI will recruit and phosphorylate downstream intracellular signal transducers: SMAD 1, 5 and 8. The phosphorylated SMAD 1/5/8 then forms a complex with SMAD4, together they translocate to the nucleus to transcribe BMP target genes. Adapted from (66).

1.4.3 Hedgehog signaling pathway

Hedgehog signaling is comprised of three major members: Indian hedgehog (Ihh), Sonic hedgehog (Shh), and Desert hedgehog (Dhh) (67). During embryogenesis, Shh and Ihh play a significant role in gut tube patterning and villus formation (68). However, in the adult SI and colon, Hh signaling is dominantly driven by secretion of Ihh with nearly undetectable levels of Shh (67). Unlike Wnt and BMP, Hh signaling is thought to occur in a paracrine fashion from differentiated epithelial cells to surrounding stromal cells (69). It is presumed that the stromal subsets responding

to Hh signals are predominantly myofibroblast and fibroblast cells, specifically localized at the crypt-villus junction of the SI or toward the top and upper-crypt regions of the colon (70, 71).

Signaling of all three Hedgehog ligands occurs through the binding to the transmembrane receptor Patched (Ptch)-1 and Ptch-2 (67). Normally, Ptch receptors inhibit an additional protein Smoothed (Smo); however, Hedgehog binding to Ptch relieves the repression, activating the downstream signaling cascade (67). This results in the activation of transcription factors, Glioblastoma (Gli) 1, 2, and 3 (67) (**Figure 6A**).

It is understood that Ihh signaling directly promotes differentiation of certain stromal subsets. Indeed, epithelial-specific Ihh deletion through *Villin-Cre; Ihh^{fl/fl}* mice resulted in the loss of α SMA⁺ myofibroblasts at the base of the intestinal crypt (72). Conversely, constitutive activation of Ihh signaling through *Ptch1^{fl/fl}; RosaCreERT2* mice caused accumulation and overexpression of myofibroblasts (70). However, in addition to regulation of the stromal compartment, Hh also indirectly acts on homeostatic maintenance of ISC proliferation (67). Epithelial deletion of Ihh through *Cyp1a^{Cre}Ihh^{fl/fl}* mice resulted in a proliferative response of the intestinal epithelium, with lengthening of crypts and increased Wnt signaling. This is because there was a reduction of BMP signaling to the epithelium, likely due to the reduced level of stromal subsets through lack of Ihh (71). Conversely, Ihh overexpression through constitutive activation of Hh signaling pathway causes stromal cell accumulation and epithelial precursor depletion (70) (**Figure 6B**).

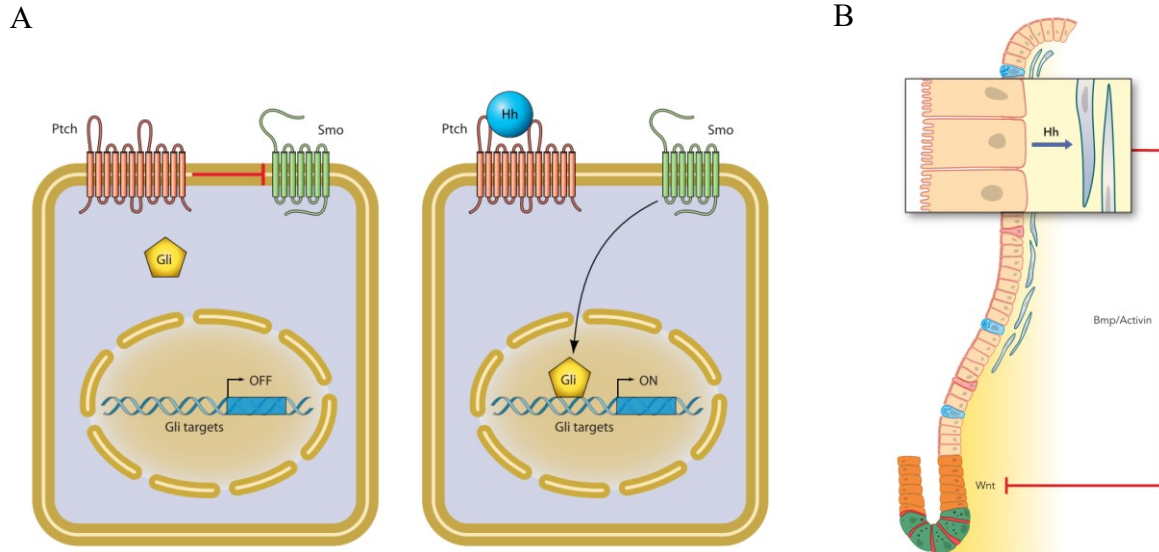


Figure 6. Hedgehog signaling pathway and negative feedback loop on ISC proliferation. (A) All three Hedgehog ligands (Sonic Hedgehog, Indian Hedgehog, and Desert hedgehog) signal through binding of transmembrane receptor Patched (Ptch)-1 and Ptch-2. When Hedgehog is not present, Ptch receptors inhibit Smoothened. However, when hedgehog is present, it will bind to Ptch and relieve its repression of Smo activating downstream transcription factors Glioblastoma 1, 2, and 3. Adapted from (67). (B) Hedgehog signaling from differentiated epithelial cells induces BMP-secretion of adjacent stromal cells. BMP will then go on to inhibit Wnt signaling to mediate ISC proliferation. Loss of Ihh results in proliferation of the intestinal epithelium, lengthening crypts and increased Wnt signaling.

1.4.4 Notch signaling pathway

Notch signaling occurs through cell-cell interactions, where one cell presents a Notch ligand (Delta, ex. DLL1 or DLL4) to an adjacent cell expressing a Notch receptor (ex. Notch1-4) (20, 73). Both the ligand and receptor are transmembrane proteins; therefore, Notch signaling acts within a short range and requires direct membrane contact between the two cells (7). Upon ligand-receptor signaling, Notch intracellular domain (NICD) is released by γ -secretase and translocates to the nucleus. Nuclear NICD then binds to the transcription factor CSL which initiates transcription of Notch target genes (73). The Notch pathway regulates two critical functions in intestinal epithelium homeostasis: (1) mediating the balance between progenitor fate of absorptive versus secretory lineages and (2) maintaining the stem cell pool (74).

Notch signaling will regulate absorptive and secretory differentiation through transcription factors, Hes1 and Atoh1 (73). A critical determinant of secretory fate is expression of the transcription factor Atoh1. However, downstream of Notch activation, transcription of target gene Hes1 becomes upregulated and directly inhibits Atoh1 activity. Thus, Notch activation pushes cells into an absorptive fate and blocks differentiation into the secretory lineage (74). Constitutive

activation of the Notch pathway through epithelium specific NICD transgene expression results in a complete loss of secretory cells (75).

Notch signaling results in a binary “on” and “off” system known as lateral inhibition, whereby cells directly adjacent to one another have opposite fate (20). A cell expressing Notch ligand (Delta) will have the capability to activate Notch signaling in neighboring cells. However, the cell receiving the Notch signaling will repress its own production of Delta, rendering them unable to activate Notch in other neighboring cells (74) (**Figure 7**). Therefore, through lateral inhibition in the TA compartment, cells with activated Notch signaling will differentiate into the absorptive lineage and limit activation of Notch in neighboring cells, pushing them to a secretory lineage (74).

Notch signaling also promotes proliferation, thus *Lgr5*⁺ ISC are generally Notch-high. Within the stem cell compartment Paneth cells will express Notch ligands DLL4 and DLL1, inducing Notch activation in ISCs (74). However, a finding showed that Paneth cells were dispensable *in vivo*, likely indicating other sources of Notch ligands are available to support ISC maintenance (76).

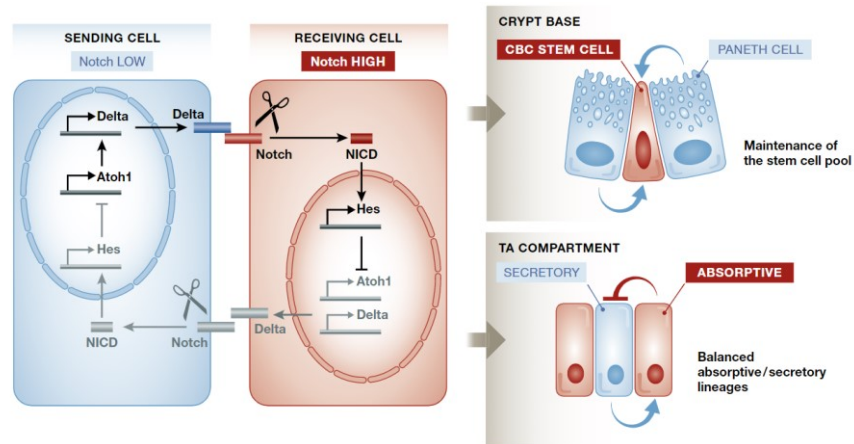


Figure 7. Notch signaling and lateral inhibition in stem cells and TA compartment. Notch signaling occurs through cell-cell contact and becomes initiated through expression of Delta ligand. Delta ligand will bind to the Notch receptor on an adjacent cell. Within the adjacent cell γ -secretase will cleave the Notch intracellular domain (NICD) allowing it to translocate to the nucleus. Here, nuclear NICD relieves repression of Notch target genes, for instance Hes family genes. Notably Hes expression determines the final fate of the cell: proliferation in the case of a stem/progenitor cell or differentiation between absorptive or secretory phenotype in TA cells. Adapted from (74).

1.5 Stromal cells

Stromal cells are characterized as a group of non-hematopoietic, non-epithelial cell types that make up and maintain connective tissue throughout the body (3). Within the intestinal connective tissue, stromal cells reside in the lamina propria between the intestinal epithelial monolayer and smooth muscle layers (47, 77). Notably, the term stromal cell encompasses a vastly heterogeneous and plastic population of subtypes (78).

Historically, understanding the heterogeneity of these populations was limited, due to reliance on less advanced imaging techniques and ambiguous molecular markers. Thus, the classification of stromal cell subsets was of low resolution, where fibroblasts, myofibroblasts, and pericytes were the only well-defined populations (3). A major issue in distinguishing between stromal subsets lies within the significant overlap of their molecular marker expression, preventing adequate delineation of cell-type specific functions (79, 80). Only recently, insight into the cellular composition of the stromal compartment has significantly improved due to the increased accessibility to single-cell RNA sequencing (scRNA-seq), Cre-driver mouse models, fine-resolution microscopy, organoid co-cultures, and fluorescence-activated cell sorting (FACS) (11). Currently, stromal cells are characterized into more refined subsets including fibroblasts, myofibroblasts, trophocytes, telocytes, and pericytes (78). However, discovery of new stromal subsets continues, and these broad classifications are dynamically changing.

Each population has a relatively distinct localization, function, and phenotype within the intestinal lamina propria. Specifically, myofibroblasts, telocytes, and trophocytes are increasingly recognized as important sources of Wnts, RSPOs, BMP ligands and antagonists (11, 78, 81). Together, they create gradients of these deterministic signals to orchestrate the architecture of the ISC niche and epithelial lineage differentiation along the crypt-villus or crypt axis (11). Notably, our understanding of the cellular sources creating the BMP gradient along the crypt-villus axis is much more well defined than our understanding of Wnt signaling. Recently, McCarthy et al. demonstrated two spatially distinct cell populations at opposite ends of the crypt axis, whereby one population provides BMP ligands at the villi or crypt-apex, and the other opposes these signals with BMP inhibitors at the crypt base (78). However, the specific cellular sources of Wnt ligands and inhibitors continues to be debated. There is an increased understanding of the redundancy within Wnt signaling sources, as several stromal subsets show ability to secrete canonical and non-

canonical Wnts. Thus, the cellular basis for Wnt signal polarity continues to be uncovered (discussed in sections below) (82).

Overall, much progress has been made in understanding the intestinal stromal composition under homeostasis in recent years; however, more studies are still necessary to elucidate the role of stromal subsets in modulating damaged epithelium under inflammatory and infectious conditions.

1.5.1 Fibroblasts

Intestinal fibroblasts are the dominant stromal cell population dispersed throughout the connective tissue of the lamina propria (3, 11). They are phenotypically non-contractile cells and a central producer of the extracellular matrix (ECM) components contributing to tissue structure and maintenance (3). Morphologically, fibroblasts are observed to have two distinct phenotypes depending on their activation state. At rest, they are spindle shaped with slender cytoplasmic processes. However, when activated, their cytoplasm becomes enlarged through an abundant rough endoplasmic reticulum and prominent Golgi, preparing for the synthesis of ECM molecules like collagens, proteoglycans, and fibronectin (3, 11)

Historically, the molecular markers used to identify intestinal fibroblasts were CD90 and vimentin, with the absence of desmin and alpha smooth muscle actin (α SMA) (3). Since then, vimentin has been understood as a pan-fibroblast marker, and such identification methods for fibroblasts was not discriminatory for the other smaller stromal subsets. More recently, expression level of platelet-derived growth factor receptor alpha (PDGFR α) has been used to help distinguish stromal subsets in conjunction with defining markers. It is understood that there is increased PDGFR α expression amongst stromal cells located near the villus and crypt apices, while PDGFR α expression decreases moving down the crypt axis (78). Indeed, while there is currently no widely accepted form of defining fibroblasts yet, an improved method proposed by McCarthy et al. is identifying the known stromal subsets then sub-setting out PDGFR α ^{lo}Cd81⁻ cells (11, 78).

1.5.2 Myofibroblasts

Myofibroblasts are frequently described as sharing phenotypic characteristics of both fibroblasts and smooth muscle cells (47). Morphologically they are thin, spindle-shaped cells, located adjacent to the intestinal epithelium and lining the entire crypt-villus or crypt axis (3). Owing to their characteristic as intermediaries between fibroblasts and smooth muscle cells, they

express pan-fibroblast markers like vimentin and CD90, but are distinguished from fibroblasts through their expression of smooth muscle markers like α SMA⁺ and heavy chain myosins (ex. *Myh11*) (83, 84). Notably, myofibroblasts are distinct from smooth muscle cells, as they lack expression of smooth muscle marker desmin, and the extent of α SMA expression is at a much lower level compared to the submucosal muscle cells (85).

Historically, myofibroblasts were regarded as the dominant stromal source of many trophic factors like Wnts, BMPs, and BMPi to maintain the intestinal epithelium (3). However, in recent years, new findings uncovered several additional niche subsets as dominant and alternative sources for these trophic factors. For instance, in 2007 Kosinski et al. initially identified myofibroblasts and smooth muscle cells underlying the crypt as the cellular sources for BMP inhibitors, *Grem1*, *Grem2*, and *Chordin-like-1* (61). However, new evidence reveals trophocytes, a stromal subset closely associated with the stem cell niche, to be the dominant producers of *Grem1* (discussed in section 1.5.4).

Similarly, myofibroblasts were also speculated as an essential stromal source of Wnts for the maintenance of ISCs. Lei et al. previously demonstrated that subepithelial myofibroblasts, when cultured *in vitro* with small intestine organoids, were able to support ISC growth through expression of Wnts and R-spondin-1 without supplementation (86). However, it is argued that myofibroblast-derived Wnts may be necessary but not essential for *in vivo* homeostatic maintenance of the ISC niche. For instance, San roman et al. showed that myofibroblast and smooth muscle cell-specific deletion of Wnt secretion through *Porcn* in *Myh11-Cre^{ERT2}* mice caused no significant defects in crypt cell proliferation, differentiation, or Wnt target-gene expression (87). Thus, there are likely several cellular sources of Wnts and R-spondins, with certain overlaps and redundancy.

1.5.3 Telocytes

Improvements in resolving the cellular composition of the stromal compartment has allowed for identification of rarer subsets like telocytes (88). Telocytes lie directly under the intestinal epithelium and are embedded in the basement membrane, enveloping the crypt-villus axis of the small intestine, and the crypt axis of the colon (11). Morphologically, they are recognized as long, thin expansive cells with telopodes extending hundreds of micrometers, allowing one telocyte to be in close contact with dozens of epithelial cells (89–91).

Several groups have independently identified such cells, with various markers used to characterize them including *Foxl1*⁺, *Pdgfra*^{High}, *Gli1*⁺, and *Cspg4*⁺ (81, 82, 92, 93). Notably, few of these markers are truly restricted to this stromal subset and are often used in combination with microscopy to assess their localization and morphology. While the population of *Foxl1*⁺*Pdgfra*^{hi} telocytes are distributed rather homogeneously along the crypt-villus axis, they tend to concentrate at higher numbers in the crypt-villus junction of the SI or middle of the colonic crypt (78, 91).

Numerous studies pinpoint telocytes as critical sources for trophic factors involved in both crypt maintenance and epithelial cell differentiation. For instance, telocytes are an important cellular source of canonical Wnts (Wnt2b) and non-canonical Wnts (such as Wnt4, Wnt5a, and Wnt5b). In *Foxl1*-hDTR transgenic mice, diphtheria toxin-mediated ablation of *Foxl1*⁺ telocytes resulted in shortening of the total SI and colon length, reduced jejunal villus and colonic crypt length, accompanied by dramatic reduction in epithelial proliferation (81). Additionally, upon *Foxl1*⁺ telocyte ablation, nuclear β -catenin levels were greatly reduced in crypts, indicating the loss of canonical Wnt signaling activity (81). Indeed, *Foxl1*⁺ telocytes are required for ISC niche maintenance and proliferation. Follow-up studies with *Foxl1*⁺ cell specific deletion of Wnt secretion using *Porcn*^{fl/fl} mice resulted in impaired proliferation of ISCs (91). Surprisingly, despite their essential role in ISC niche maintenance, when telocytes were isolated and co-cultured with intestinal crypts, they were unable to maintain organoid growth (78). In addition to Wnts, telocytes are dominant producers of BMPs (like *Bmp2/4/5* and the sole source of *Bmp7*) contributing to the maintenance of the BMP gradient, and thus epithelial cell differentiation (78). As telocytes are distributed throughout the crypt-villus axis at various densities, their role at the villus tips of the SI and crypt apex of the colon is not well characterized. It is speculated that they could play a role in anoikis; however, this still remains to be explored (78).

1.5.4 Trophocytes

The most recently identified stromal cell population are trophocytes, located at the base of the intestinal crypt compartment in close contact with ISCs (78). They are sub-setted out from *PDGFR α* ⁺ cells as *PDGFR α* ^{lo} expressors, and further differentiated from *PDGFR α* ^{lo} fibroblasts through the expression of *CD81*⁺ (78). In conjunction with their close proximity to the stem cell niche, trophocytes directly support the maintenance of ISCs. Notably, they are prominent producers of the BMP inhibitor, *Grem1* and counteract the gradient of BMPs generated from

telocytes. Such counteracting gradient helps maintain stemness of the compartment and proliferative capacity of ISCs, simultaneously inhibiting pro-differentiation BMP signals. Their capacity to support ISC growth and stemness is further validated by co-cultures of trophocytes alone with organoids. Here, selective omission of organoid cocktail media – Wnt, Rspo1, BMPi, and EGF still resulted in ISC survival. This is because trophocytes are known producers of canonical Wnt ligand, Wnt2b, as well as Rspo1 and Rspo2, that help maintain stemness of ISCs (78). Although the identification of trophocytes is extremely recent, this stromal subset was also similarly described by at least two other independent groups (94, 95).

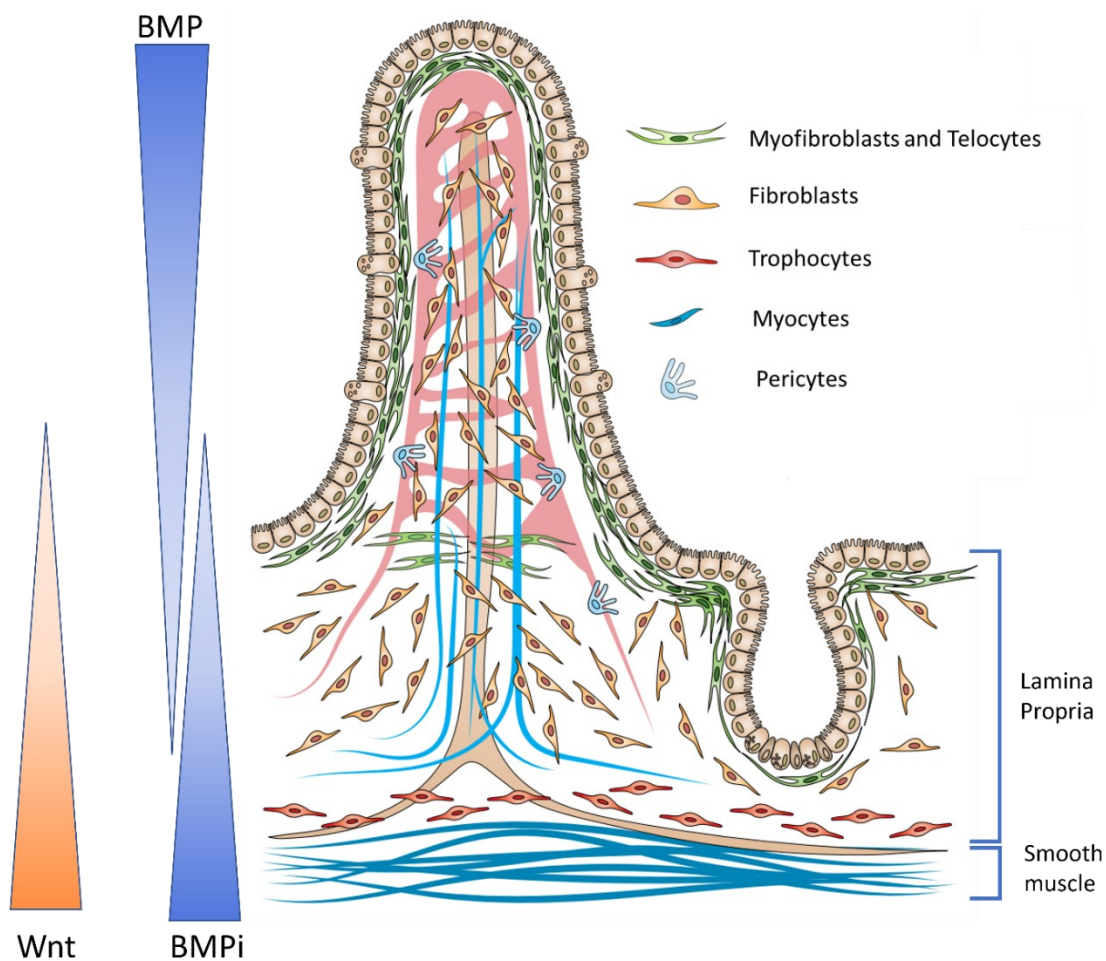


Figure 8. Intestinal stromal subset localization and distribution within the crypt compartment. The stromal compartment within the intestinal lamina propria contains several well-defined subsets including myofibroblasts, telocytes, fibroblasts, trophocytes, and pericytes. Myofibroblasts and telocytes (green) underlie the intestinal epithelium throughout the crypt-villus axis of the SI and the crypt axis of the colon. Fibroblasts (orange) are broadly distributed throughout the lamina propria. Trophocytes (red) are concentrated at the base of intestinal crypts, secreting BMPi like *Grem1* to promote Wnt signaling and the ISC niche. Pericytes (light blue) line the lymphatic and blood vessels. Myocytes (dark blue) lie parallel to the smooth muscle layer.

1.6 Disruption of homeostasis during intestinal inflammation and infection

As previously reviewed, the intestinal environment is tightly regulated under homeostasis. However, this balance can be skewed through exposure to intestinal pathogens, insult, or injury, risking the destruction of mucosal and epithelial barriers and exposing host tissue to the harsh luminal environment. The intestine must therefore be equipped with appropriate repair mechanisms. While many have investigated the epithelial and immune responses to intestinal disruption, little is known about how the intestinal stromal compartment aids in the response to infection and inflammation. Several examples of inflammatory diseases and infectious models relevant to our work are described below.

1.6.1 Inflammatory Bowel Disease

Inflammatory bowel disease (IBD) is a chronic inflammatory disease of the GI tract with two main forms: Crohn's disease and ulcerative colitis (UC) (96). In recent years, many advances have been made in understanding the etiology of IBD. Susceptibility of a host is suspected to be a combination of genetic predisposition, microbial factors, environmental factors, and immune mediated tissue damage (97).

While they are both forms of IBD, Crohn's disease and UC differ in their localization and pathophysiology. Crohn's disease affects any part along the GI tract from the mouth to the anus; however, most cases involve the ileum and colon (97). A key histopathologic characteristic for Crohn's is transmural inflammation, meaning it can affect all layers of the intestinal wall – beginning from the mucosa and penetrating into the serosa (98). Consequently, the clinical manifestations include abdominal pain, fever, diarrhea with blood and/or mucus, and clinical signs of bowel obstructions (96, 99). In contrast, UC is restricted to the colon, generally beginning at the rectum and extending proximally through the colon (96). Histopathologically, UC is confined to the mucosa and submucosa, resulting in extensive superficial mucosal ulcerations with significant infiltration of neutrophils to the colonic crypts (96, 98). Symptoms of the disease may manifest as bloody diarrhea, rectal bleeding, abdominal pain during bowel movements, weight loss, and fatigue (96).

Barrier function is crucial to the maintenance of intestinal homeostasis. However, in IBD patients increased intestinal permeability and defects in barrier function are highly prevalent (100–102). Analysis of human IBD biopsies indicated decrease of junctional proteins like E-cadherin

and β -catenin, resulting in reduced integrity of the mucosal barrier (96). The widely believed hypothesis is that in genetically susceptible individuals, epithelial barrier disruption instigates the disease. A subsequent loss of immune tolerance to intestinal antigens triggers a cascade of pro-inflammatory immune responses (89).

While the intestinal epithelium and immune system are highly implicated in the response to IBD, recent reports also suggest that IBD induces structural remodeling of the stromal microenvironment in response to chronic inflammation (80, 103). Kinchen et al. demonstrated significant and consistent alterations in the stromal microenvironment of DSS-treated mice and IBD patient biopsies compared to healthy controls (80). Through scRNAseq, they identified specific stromal populations that correlated with healthy versus inflammatory status. Specifically, under homeostasis they identified a niche $CD142^+SOX6^+$ stromal population. This population was enriched with essential Wnt genes, localized in proximity to intestinal crypts, and believed to maintain the crypt compartment. However, under inflammatory conditions the stromal compartment underwent a significant remodeling event with a decline of $CD142^+SOX6^+$ cells, accompanied by an upregulation of a pro-inflammatory $IL33^+CCL19^+$ stromal population secreting IL-6 and TNFSF14. This pro-inflammatory stromal response also promoted increased T-cell recruitment, redox imbalance, and epithelial barrier breakdown (80).

Similarly, through scRNAseq analysis and genome-wide association studies, Smillie et al. mapped cell types associated with UC, noting significant remodeling events of the stromal, epithelial, and immune environment under chronic inflammation (103). Within the stromal population, they observed significant expansion of a stromal subset they have termed inflammatory-associated fibroblasts, which expanded up to 189-fold in the inflamed tissue of UC patients (103). This population is marked by many genes associated with colitis, fibrosis, and cancer, like *Il11*, *Il24*, and *Il13ra2*. In addition, the stromal remodeling event was accompanied by epithelial and immune cell remodeling. Specifically, UC patient samples showed an expansion of a microfold-like cell population which highly expressed chemokines *CCL20* and *CCL23*, suggesting involvement in immune cell recruitment. Likewise, there was an expansion of $CD8^+IL-17^+$ T cells and T_{regs} which provided major sources of *Il-17* and *TNF*, respectively (103). Together, these data show significant remodeling events occur in the intestinal lamina propria during inflammatory conditions.

1.6.2 Enteropathogenic and enterohemorrhagic *Escherichia coli*

Escherichia coli is a Gram-negative bacterium belonging to the *Enterobacteriaceae* family (104). It exists as a dominant facultative anaerobe in the commensal microbiota of the intestine and is generally avirulent to a healthy host (104). However, several pathogenic *E. coli* strains have acquired virulence attributes, allowing them to cause a broad spectrum of disease in humans (105, 106). These pathogens are categorized in six major pathotypes based on their virulence properties: enteropathogenic *E. coli* (EPEC), enterohaemorrhagic *E. coli* (EHEC), enterotoxigenic *E. coli* (ETEC), enteroinvasive *E. coli* (EIEC), enteroaggregative *E. coli* (EAEC), and diffusely adherent *E. coli* (DAEC) (104, 107). Specifically, EPEC and EHEC are an important cause for morbidity and mortality worldwide (108). They share a unique mechanism of colonization in which they intimately adhere to the intestinal epithelial membrane.

EPEC colonizes the SI and causes profuse watery diarrhea. While EPEC infection is rather limited in developed countries, it is still a major cause for diarrhea in infants younger than two in developing countries (107). In contrast, EHEC is a distinct class of pathogenic *E. coli* infecting the colon rather than the SI as seen in EPEC. An additional defining feature is the production of Shiga-toxin (Stx), a highly potent toxin that results in hemorrhagic colitis (104, 106). EHEC is also characterized by severe abdominal pain, accompanied by bloody diarrhea, non-bloody diarrhea, and hemolytic uremic syndrome (104).

A hallmark of EPEC and EHEC histopathology is formation of attaching-and-effacing (A/E) lesions, whereby the bacteria intimately adhere to the epithelial surface, followed by effacement of the host brush border microvilli (104, 106). These A/E lesions are detectable at an ultra-structural level and their formation relies specifically on a conserved pathogenicity island called the locus of enterocyte effacement (LEE) (104). The LEE encodes a type III secretion system (T3SS) as well as effectors critical for pathogenesis, like intimin and translocated intimin receptor (Tir). During early infection, loosely adherent *E. coli* will translocate Tir into the infected enterocyte through the T3SS. Tir then acts as a receptor for outer membrane adhesin intimin.

EPEC and EHEC strains also characteristically alter the host cytoskeleton through actin polymerization, forming a pedestal structure extending outward from the cell upon which the bacterium sits (104). Additionally, other pathology includes extensive villus atrophy and thinning

of the mucosal lining (105). While the infection greatly involves the mucosa and submucosa, little information is available on the stromal-specific response to *E. coli* infection.

1.6.3 *Citrobacter rodentium*

While EPEC and EHEC represent important *E. coli* pathotypes in human disease, these A/E pathogens cannot be directly modeled in mice as they are naturally resistant to infection (109). However, *Citrobacter rodentium* is a mouse-specific, gram-negative mucosal pathogen, considered an excellent tool to study the molecular basis and mechanisms of A/E pathogens (110). Specifically, *C. rodentium* shares several key pathogenic mechanisms with EPEC and EHEC including the same LEE-related genes and effectors required to form A/E lesions (109). In addition, *C. rodentium* has been used as a model to study other intestinal disorders such as IBD, infectious colitis, and tumorigenesis as its pathogenic characteristics involve epithelial barrier integrity, mucosal healing, intestinal inflammation, and epithelial hyperproliferation (110).

Genetic background of the mice greatly influences susceptibility to *C. rodentium* infection and disease severity (111). Infection in resistant mouse strains, like C57Bl/6, leads to mild, self-limited colitis, which is cleared after several weeks (109). Generally, pathology is characterized by the thickening of the mucosa and the characteristic development of colonic crypt hyperplasia (CCH). CCH occurs when colonic crypts become lengthened due to extensive proliferation of TA cells, which typically lasts 2-3 weeks (109). In contrast, our group along with several others have identified multiple strains of hyper-susceptible mice that develop severe pathogenesis and succumb to lethal diarrhea, including C3H/HeJ, C3H/HeOuj, FVB, and AKR/J mice (111, 112). Here, pathology is associated with significant CCH proliferative response of the colonic crypts along with poor differentiation of enterocytes and goblet cells. Loss of enterocyte differentiation results in impaired ion exchange, affecting electrolyte absorption and profuse diarrhea-inducing death (113). Through genetic linkage analysis studies, we have demonstrated that susceptibility to *C. rodentium* infection is controlled by the *Cri* locus on chromosome 15 which encompasses the *Rspo2* gene (113).

Rspo2 is one of four R-spondins (*Rspo1-4*) produced by the stromal compartment which act as potent enhancers of the canonical Wnt signaling pathway (114). In susceptible mice, a genetic haplotype upstream of *Rspo2* drives high levels of *Rspo2* signaling leading to the pathological activation of Wnt signaling, triggering the loss of epithelial cell differentiation (115).

The cellular source responsible for this event was speculated to be sub-epithelial myofibroblasts; however, these findings were prior to the finer resolution of the stromal cell subsets. Indeed, other stromal cells may be involved in mediating this hyperproliferative crypt response. Likewise, there is extensive remodeling of the intestinal mucosa and epithelium in response to *C. rodentium* infection, yet little is known about how the stromal cell compartment may be remodeling in conjunction.

1.7 Hypothesis

Currently, understanding of the intestinal stromal cell compartment goes beyond a passive structural role. As described above, heterogeneous stromal subsets provide essential signaling cues and structural support to the intestinal epithelium, demonstrating significant involvement in intestinal homeostasis maintenance. However, less is understood about stromal cell contribution to intestinal health during inflammation and infection. Early studies demonstrate that stromal cells undergo remodeling events in response to specific types of chronic intestinal inflammation, but more work is needed to elucidate their response to intestinal infection, and how they promote intestinal epithelial recovery. Therefore, we hypothesize that under infectious and inflammatory conditions, stromal cells contribute to intestinal remodeling and drive regenerative signaling to promote epithelial repair.

Our specific aims are as follows:

Aim 1: Analyze the response of the intestinal stromal cell compartment following enteric infection.

Aim 2: Determine the ability of stromal cell secreted factors to mediate intestinal epithelial phenotype in inflammation and regeneration

CHAPTER 2: MATERIALS AND METHODS

2.1 Experimental animals

Breeding and handling of DAT^{tdTomato}, *Cd109* KO, Clu^{tdTomato}mPGES-1-KO, and littermate controls were conducted in accordance with the Canadian Council of Animal Care (CCAC) approved by McGill University Animal Care Committee (MUACC). Mice were anesthetized with isoflurane then euthanized with CO₂.

2.2 Gut Preparation

Colon samples were prepared for scRNAseq, as previously described. Briefly, colons were harvested, the feces were removed, and the colon was placed into ice-cold Gut-buffer (HBSS (Gibco: 14175), supplemented with 2% FCS (10 ml/500 ml), 15mM HEPES (7.5 ml/500 ml) (Gibco: 15630)). Following, the colon was cut into 1-2 cm pieces, placed into HBSS-EDTA buffer (HBSS (Gibco: 14175), 2% FCS (10 ml/500 ml), 15mM HEPES (7.5 ml/500 ml) (Gibco: 15630), 1 g EDTA/500 ml; buffered to pH 7.3) at RT, and vortex vigorously to remove luminal contents. The wash was then repeated with fresh HBSS-EDTA. Colon pieces were then transferred into 5 mL LP-digestion buffer (RPMI-1640 (Sigma: R0883), 10% FBS (50 ml/500 ml), 15 mM HEPES (7.5 ml/500 ml) (Gibco: 15630)). 60 µL of digestive enzyme mix (40 µL collagenase IV and 20 µL DNase I) was added to the LP-digestion buffer and incubated in a 37°C water bath for 30 minutes. Notably, the tissue was vortexed every 15 minutes. Upon completion of the first digestion, the gut pieces were re-digested for another 30 minutes with fresh LP-digestion buffer with digestive enzyme mix. Cells were then pelleted, resuspended in 3 mL of FACS buffer, then live cells were sorted and collected by flow cytometry, and prepared for scRNAseq.

2.3 scRNAseq

scRNAseq was completed using 10x Genomics Chromium sequencing by collaborators at the Stratton Laboratory. Colonic lamina propria cells were isolated and pooled from three B6.129 mixed background mice for each group (3 uninfected, 3 *C. rodentium* infected). Using the Single Cell 3' Reagent kit (V3.1 assay, <https://www.10xgenomics.com/support/single-cell-gene-expression>), 40 000 cells were loaded on the Chromium per the manufacturer's instructions. Reverse transcription (RT), cDNA synthesis and amplification, and library preparation were completed by collaborators in the Stratton laboratory. In brief, cells were first partitioned on a nanoliter-scale using barcoded Gel Bead-In-Emulsions (GEMs). Following GEM generation, Gel

Beads are dissolved, primers were released, and co-partitioned cells were lysed. Cellular transcripts were then reverse transcribed with primers containing (1) TruSeq sequence, (2) 16 nt 10x Barcode, (3) a 12nt unique molecular identifier (UMI), and (4) a 30 nt poly(dT) sequence, which becomes mixed with the cell lysate and Master Mix containing RT reagents. The incubation resulted in barcoded, full-length cDNA from poly-adenylated mRNA. Following, Silane magnetic beads were used to purify the cDNA from the RT reaction mixture, then cDNA was amplified through PCR, generating a library. Sequencing was performed using NovaSeq 6000 S4 PE 100bp, resulting in a final output of on average, 20 000 reads/cell, which are then processed using 10X Genomics Cell Ranger. FASTQs output were aligned to the mouse GRCm38.p5 reference genome. Each sample has been assigned Gene-Barcode matrices by counting UMIs and filtering non-cell associated barcodes. Finally, Seurat V4.0.6 R toolkit was used for quality control and downstream analysis of the single cell RNAseq data. Each Seurat object was identified with default parameters (min. cells = 3, min. features = 200) and low-quality cells were excluded based on gene counts and % of mitochondrial genes (downstream analyses were performed on cells with gene counts between 200 and 2500, and mitochondrial genes < 5%). Gene expression was log normalized to a scale factor of 10 000. Both Seurat objects (uninfected and infected) were then integrated as previously described in Stuart, Butler et al. 2019 (116).

2.4 *C. rodentium* infection

Prior to the infection, chloramphenicol resistant *C. rodentium* was grown in 3 mL of Luria-Bertani (LB) broth overnight at 37°C with shaking. Mice were infected by oral gavage with 0.1 mL of LB broth containing 2-3 x10⁸ CFU of bacteria. They were monitored daily and weighed every two days. The DAT^{tdTomato} mice were harvested on days 6 and 13, the *Cd109* WT and KO mice were harvested on day 13. To evaluate the infectious burden of *Cd109* WT and KO mice, their feces were collected at d4, d6, and d12 timepoints post infection, serially diluted in PBS, and plated onto MacConkey agar supplemented with chloramphenicol. The Petri dishes were incubated at 37°C, and colonies were counted on the following day. Infected mice with no detectable colonization were removed from the experiment. Percent body weight and CFU were graphed using GraphPad prism v 9.2.

2.5 Lineage tracing experiments in irradiated intestine of mice

Lineage tracing of Clu⁺ cells and progeny was initiated with TAM injection in Clu^{tdTomato} mPGES-1 WT and KO mice. On d1 Clu^{tdTomato} cells were marked with 2.5 mg TAM injection, followed by whole body irradiation on d2 at 12 Gy using X-RAD SmART Irradiator. On d7 the small intestines were collected and fixed in 10% buffered formalin for FFPE processing.

2.6 DSS treatment

Mice were administered 2.5% DSS (Alfa Aesar, J63606) in their drinking water. The mice were treated with DSS for 5 days, then switched to normal drinking water until euthanized. Their weights were monitored daily, and mice were euthanized when body weight dropped below 80% of their starting weight.

2.7 Primary stromal cell cultures

Primary stromal cells were isolated from the SI of 3–4-week-old, C57BL/6 background mice. Mice were euthanized and the midsection of the SI was harvested and placed in cold phosphate buffered saline (PBS). Using a syringe, the interior of the intestine was flushed with cold PBS to remove luminal contents. Next, the tissue was opened longitudinally and washed four times with cold PBS, refreshing with new PBS each wash. The tissue was then placed in a 5 mM PBS-EDTA solution, incubated at 4°C with horizontal shaking for 40 minutes, transferred into a 50 mL conical tube containing PBS. The tube was thoroughly agitated to detach the epithelial crypts. This was repeated two more times, discarding the supernatant, and refreshing with new PBS each time, until the tissue was floating in solution – indicating that the intestinal crypts were dissociated. Next, the tissue was shredded into small fragments using a scalpel and incubated in 5 mL of Advanced DMEM-F12 medium (Gibco, 11995-065) containing 50 µg/L Liberase (Sigma Aldrich, 5401135001) at 37°C for 50 minutes. The tube was agitated through manual shaking every 10 minutes. An additional 5 mL of Adv. DMEM/F12 + 10 % FBS was added to neutralize the Liberase. The contents were then centrifuged for 5 minutes at 167 RCF and was resuspended in 10 mL of Advanced DMEM/F12 (Gibco, 12634-010) supplemented with 2 mM GlutaMAX (Gibco, 35050-061), 10 mM HEPES (Gibco, 330-050-EL), 10% FBS, 100 U/mL Penicillin/100 µg/ml Streptomycin (Wisent, 450-201-EL). Following, the cells were transferred into a 60 mm dish (Corning) and incubated at 37°C with 5% CO₂. The next day the media was changed, and

subsequently the cells were passaged and split when they reached 80-90% confluency. For stimulations, 200,000-300,000 cells/well were seeded in a 12 well plate.

2.8 Immunohistochemistry and immunofluorescence

Immunohistochemistry (IHC) and Immunofluorescence (IF) staining was completed on SI and colon tissue that was formalin-fixed paraffin-embedded (FFPE), then cut into 5 μm cross sections.

To complete the IHC stainings, slides were first deparaffinized with xylene and then gradually dehydrated in ethanol (progressing from 100%, 90%, then 80% solutions). Antigen retrieval was completed in a vegetable steamer (Hamilton Beach, 37530C), where slides are first dipped into boiling dH_2O for 10 seconds, then transferred to a 1x solution of citrate buffer (Sigma Aldrich, C9999) (pH 6). Slides were then transferred into a 3% solution of H_2O_2 for 15 minutes to remove endogenous peroxidase activity, then rinsed with PBS. A hydrophobic barrier was drawn circling the tissue using the ImmEdge hydrophobic pen (Vector Laboratories, H-4000), then incubated in a 1%-bovine albumin serum (BSA)-PBS solution for 2-2.5 h in a humidity chamber to block nonspecific antibody binding to the sample. This was followed by the primary antibody incubation overnight at 4°C. The next day, the slides were washed for 20 minutes in an EasyDip™ Slide Staining Jar (Fisher Scientific, 5300) filled with PBS, with manual shaking every 5 minutes. The wash step was repeated 2 additional times. The tissue was then incubated with a detection antibody (Anti-rabbit envision secondary antibody, refer to table 1) for 1.5 h in a humidity chamber. Slides were washed with PBS three times, as previously indicated. DAB colour development solution (Sigma Aldrich, D3939) was then used to visualize the detection antibody, followed by a counterstain by dipping the slides in hematoxylin dye for 10 seconds (Eprelia, 7221). The slides were then mounted with a cover slip using Permount mounting medium (Fisher Chemical, SP15-100). Samples were analyzed with a brightfield microscope.

The IF staining procedure was similar to IHC for the deparaffinization, antigen retrieval, and BSA-blocking. However, H_2O_2 treatment was not performed. After the 1% BSA-PBS block and primary antibody incubation overnight, the slides were washed with PBS and incubated with a fluorescent detection secondary antibody for 1.5 h in a humidity chamber. Following, the slides were washed three times in PBS and stained with DAPI for 30 minutes to identify the cell nuclei. To mount the slides, Fluoromount-G mounting medium (ThermoFisher, 00-4958-02) was used.

Samples were analyzed using the LSM 880 confocal microscope (Zeiss) and quantified using QuPath.

Table 1. List of Primary and Secondary antibodies used, dilutions, and catalogue information

	Antibody detection	Dilution	Supplier and Catalogue number
1 ^o	Rabbit anti-Red Fluorescent Protein (RFP)	1:500	Rockland, 600-401-379
	Mouse anti-E-cadherin	1:500	BD transduction lab, 610181
	Rat anti-Ck19 (Troma-III-c)	1:500	Developmental Studies Hybridoma Bank
2 ^o	Anti-rabbit IgG (H+L), F(ab') ₂ Fragment Alexa Fluor® 555 Conjugate	1:400	Cell Signaling, 4413S
	Anti-rabbit Envision secondary	Ready to Use	Dako, D3939
	Donkey anti-mouse 488	1:400	Invitrogen, SA5-10166
	Goat anti-rat 633	1:400	Invitrogen, A21084
Other	DAPI	1:2000	Thermo Fisher, D1306

2.9 Fluorescent *in situ* hybridization

Fluorescent *in situ* hybridization (FISH) was performed on FFPE mouse SI and colon tissue samples using the RNAscope Multiplex Fluorescent V2 Assay (Advanced Cell Diagnostics, 323100) according to the manufacturer's instructions. In brief, slides were first baked at 60°C for 1 h, then deparaffinized according to the IHC/IF procedure above. Samples were then pre-treated with RNAscope H₂O₂ for 10 minutes at room temperature, followed by antigen retrieval in Target Retrieval Reagent for 15 minutes in a steamer as described in the IHC/IF protocol. Next, a hydrophobic barrier was drawn circling the tissue using the ImmEdge hydrophobic pen (Vector Laboratories, H-4000). RNAscope protease plus was then added to the tissue sections and then incubated at 40°C in the HybEZ oven for 30 minutes. To hybridize probes, probes were first pre-warmed to 40°C and then added to the slides to be incubated at 40°C for 2h. This was followed by a 3-step signal amplification procedure for each probe-fluorescent channel pairing as per the manufacturer's directions.

To combine FISH RNAscope with IF detection, completion of the RNAscope procedure was followed immediately by the IF procedure described above, starting at the primary antibody addition step. Samples were analyzed using the LSM 880 confocal microscope (Zeiss).

Table 2. List of RNAscope probes and fluorescent fluorophores used with associated catalogue numbers.

Probe	Catalogue number
Mm-Cd109-C1	ACD, 450021
Mm-Ifi44-C3	ACD, 534531-C3
Mm-Wnt2b-C2	ACD, 405031-C2
Mm-Grem1-C3	ACD, 314741-C3
Mm-BMP2-C1	ACD, 406661
Mm-Acta2-C1	ACD, 319531
TSA plus Cy5	NEL745001KT
TSA plus Cy3	NEL744001KT
TSA plus Fluorescein	NEL741001KT

2.10 Organoid culture

Crypt-derived small intestinal organoids cultures were established as originally described by Sato et al. (12). Briefly, the SI was harvested, washed in ice-cold PBS, and incubated with 2 mM PBS-EDTA for 30 minutes at 4°C. The epithelial crypts were released from the tissue through three rounds of vigorous shaking in a 50 mL conical tube with 15 mL of PBS. The isolated crypts were then filtered through a 70 µm cell strainer, counted, and pelleted. They were suspended at 200-300 crypts per 30 µL of Matrigel Matrix (Corning, 356234) and plated in dome-like structures in 24-well plates. Upon polymerization of Matrigel, 500 µL of crypt culture media was added (Advanced DMEM/F12 (Gibco, 12634-010) supplemented with 2 mM GlutaMAX (Gibco, 35050-061), 10 mM HEPES (Gibco, 330-050-EL), 100 U/mL Penicillin/100 µg/ml Streptomycin (Wisent, 450-201-EL), N2 Supplement (1x) (Gibco, 17502048), B-27 Supplement (1x) (Gibco, 17504044), EGF (50 ng/mL) (Wisent, 511-110), Noggin (20 µL/mL, made in house), Rspo1 (20 µL/mL, made in house), and NAC (1.25 mM) (Sigma-Aldrich, A9165-25G)).

For stromal-organoid conditioned media (CM) cultures, stromal cell media was replaced with FBS-free media 24 h prior to supernatant collection. Following, 1mL of supernatant was aliquoted from confluent cultures. The CM was then supplemented according to the previously described crypt culture media, then added onto Matrigel-suspended crypts.

2.11 Quantitative real-time qPCR

For RNA isolation, organoids were lysed by dissolving Matrigel including organoids in RNA Lysis Buffer with 1%- β -mercaptoethanol (Invitrogen, 12183020). Total RNA was extracted from crypt-derived organoid cultures using the PureLink RNA Mini Kit (Invitrogen, 12183020) following the manufacturer's instructions. The purity and concentration of RNA was evaluated using a Nanodrop (Thermo). cDNA was synthesized from 500ng of RNA using the high-capacity SuperScript IV reverse transcriptase kit (Invitrogen, 11756050). Each reverse transcription reaction was run on the BioRad T100 Thermal Cycler. All mRNA expression levels were evaluated using qPCR the PowerUp™ SYBR™ Green kit (Applied Biosystems, A25742) and the MyiQ Real-Time qPCR detection system. Relative gene expression was calculated according to the $\Delta\Delta$ CT method and normalized to *Hprt* housekeeping gene. Graphs were created using Graphpad Prism v 9.2.

Table 3. List of mouse primer sequences used.

Transcript name	Primer sequences (mouse)
<i>Clusterin</i>	F: 5'-CCCCAAAGGGGGTGTACTTG-3' R: 5'-TGGACAGTTCTTGGAGCTCAT-3'
<i>Il-33</i>	F: 5'-ATCCCAACAGAAGGCCAAAG-3' R: 5'-CCAAAGGCAAAGCACTCCAC-3';
<i>Il1rn</i>	F: 5'-TGTGCCTGTCTTGTGCCAAGTC-3', R: 5'-GCCTTTCTCAGAGCGGATGAAG-3'
<i>Lgr5</i>	F: 5'-AGAGCCTGATACCATCTGCAAAC-3' R: 5'-TGAAGGTCGTCCACACTGTTGC-3'
<i>Olfm4</i>	F: 5'-GCTCCTGGAAGCTGTAGTCA-3' R: 5'-GGCCCCAGGCACCATATTTA-3'

CHAPTER 3: RESULTS

3.1 Aim 1. Analyze the response of the intestinal stromal cell compartment following infection with *C. rodentium*

3.1.1 scRNAseq analysis of the intestinal stromal compartment at d6 and 13 post *C. rodentium* infection

Due to the heterogeneous nature of the stromal cell compartment, recent advances in scRNAseq have been an asset in bettering our understanding of stromal remodeling that occurs under inflammatory or infectious conditions. To analyze these changes in stromal composition upon *C. rodentium* infection, we infected B6.129 mixed background mice via oral gavage with $2-3 \times 10^8$ CFU of *C. rodentium*. They were sacrificed at an early timepoint of infection (d6 pi) and the peak of infection (d13 pi). The lamina propria of colons were collected, processed, and our collaborators completed scRNAseq, integrating the d6 and d13 data, and sub-setting out stromal populations from immune cells.

Through unbiased clustering, we identified the well characterized stromal subsets according to the expression of their molecular markers, including: *Cd81⁺Grem1⁺* trophocytes, *Acta2⁺Myh11⁺* myofibroblasts, *Foxl1⁺Bmp7⁺* telocytes, and *Pdgfra^{lo}Sfrp1⁺* fibroblasts (**Figure 1A**). However, in addition to these clusters, we observed an unidentified cluster of stromal cells that were present only under infectious conditions, appearing transiently at d6 p.i. and non-existent at d13 p.i. (**Figure 1B-C**). We further explored the nature of this cluster. GO enrichment terms for this subset included “T cell activation” and several roles in “antigen processing and presentation”, suggesting that they may play roles in inflammatory mediation; we therefore dubbed the cluster as “Inflammatory-associated fibroblasts” (IAFs) (**Figure 1D**). According to the DEGs, these IAFs were high expressors of *Neto2*, *Cd109*, and IFN stimulated genes like *Ifi44*, *Isg15*, *Irf7* (data not shown). Together, these data indicated that *C. rodentium* infection is capable of inducing remodeling events within the stromal compartment. Additionally, *C. rodentium* may elicit the transient emergence of an IAF population.

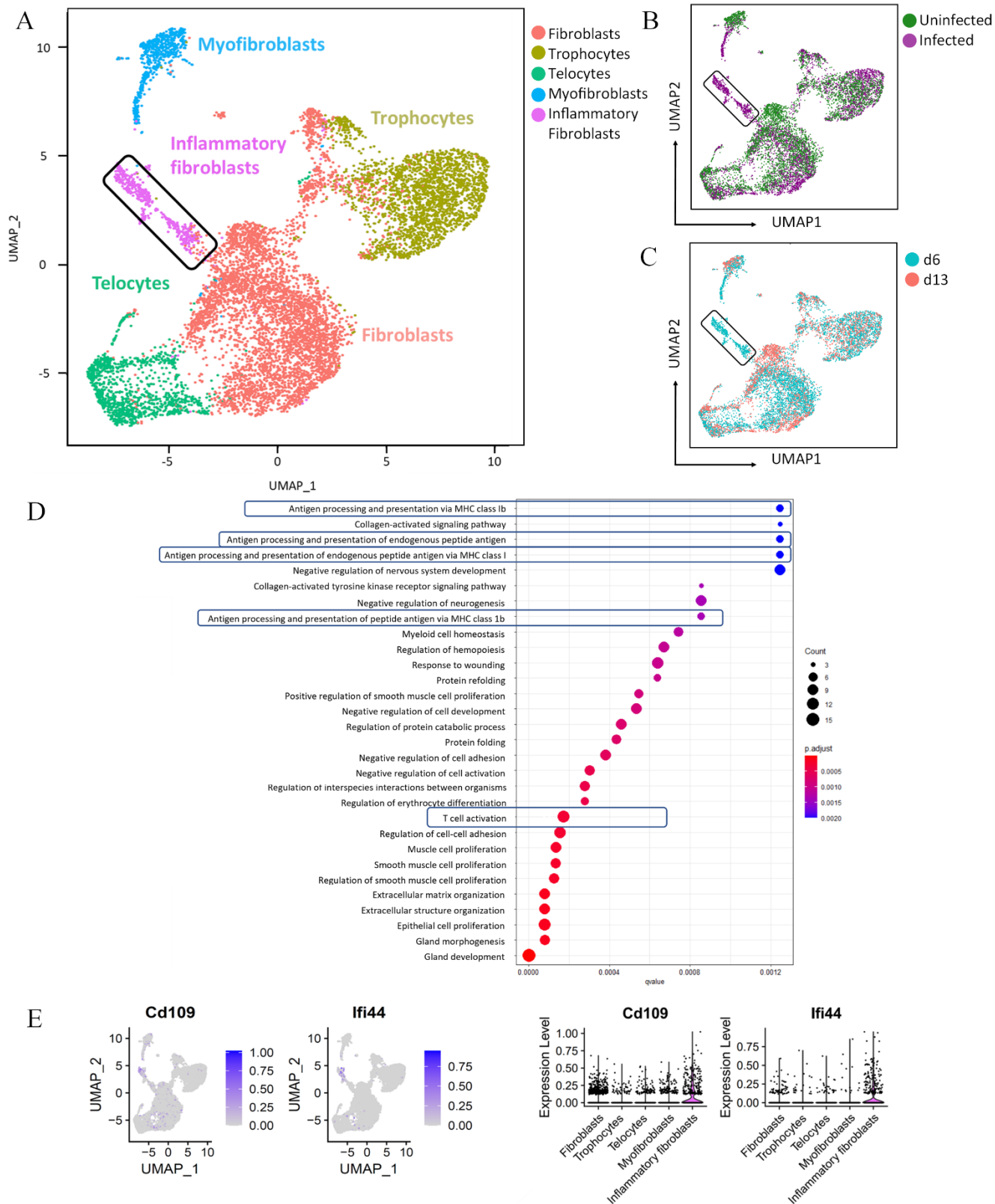


Figure 1. scRNAseq analysis of intestinal lamina propria reveals emergence of an inflammatory-associated fibroblast population at d6 post *C. rodentium* infection. (A) Discrete clustering of stromal cell subsets by UMAP analysis of RNA profiles from integrated d6 and d13 p.i. datasets. Clustering is further distinguished by (B) infection status and (C) day p.i. (D) GO terms of inflammatory fibroblast population. (E) Feature plots and corresponding violin plots depicting relative expression of *Cd109* and *Ifi44* in the inflammatory-associated fibroblast population.

3.1.2 *Cd109*⁺*Ifi44*⁺ IAFs are localized at the tops of colonic crypts and appear transiently at early timepoints of infection

Given our findings from the scRNAseq results, we wanted to confirm the emergence of the IAF population and investigate their localization through fluorescent *in situ* hybridization (FISH) and histological analysis. Based on the upregulation and specificity of *Cd109* and *Ifi44* transcripts within the IAF population (**Figure 1E**), we selected them to visualize the population histologically. Colons were harvested from uninfected and *C. rodentium* infected B6.129 mixed background mice at d0 and d6 timepoints. *Cd109* and *Ifi44* transcripts were undetectable at d0; however, in line with the scRNAseq data at d6, these transcripts were upregulated and localized at the tops of colonic crypts (**Figure 2A**). Interestingly, this phenomenon was also observed in a different mouse strain – C3H/Ouj.B6. However, here, *Cd109* and *Ifi44* transcripts were nearly undetectable at d0 and d6, and the transcripts became upregulated at d9 timepoints (**Figure 2B**). While there exists a discrepancy between the specific timepoint in which IAFs become transiently upregulated in our two mouse strains, we reasoned that the appearance of this population is a phenomenon generally occurring at early timepoints of infection, leading up to the peak of infection.

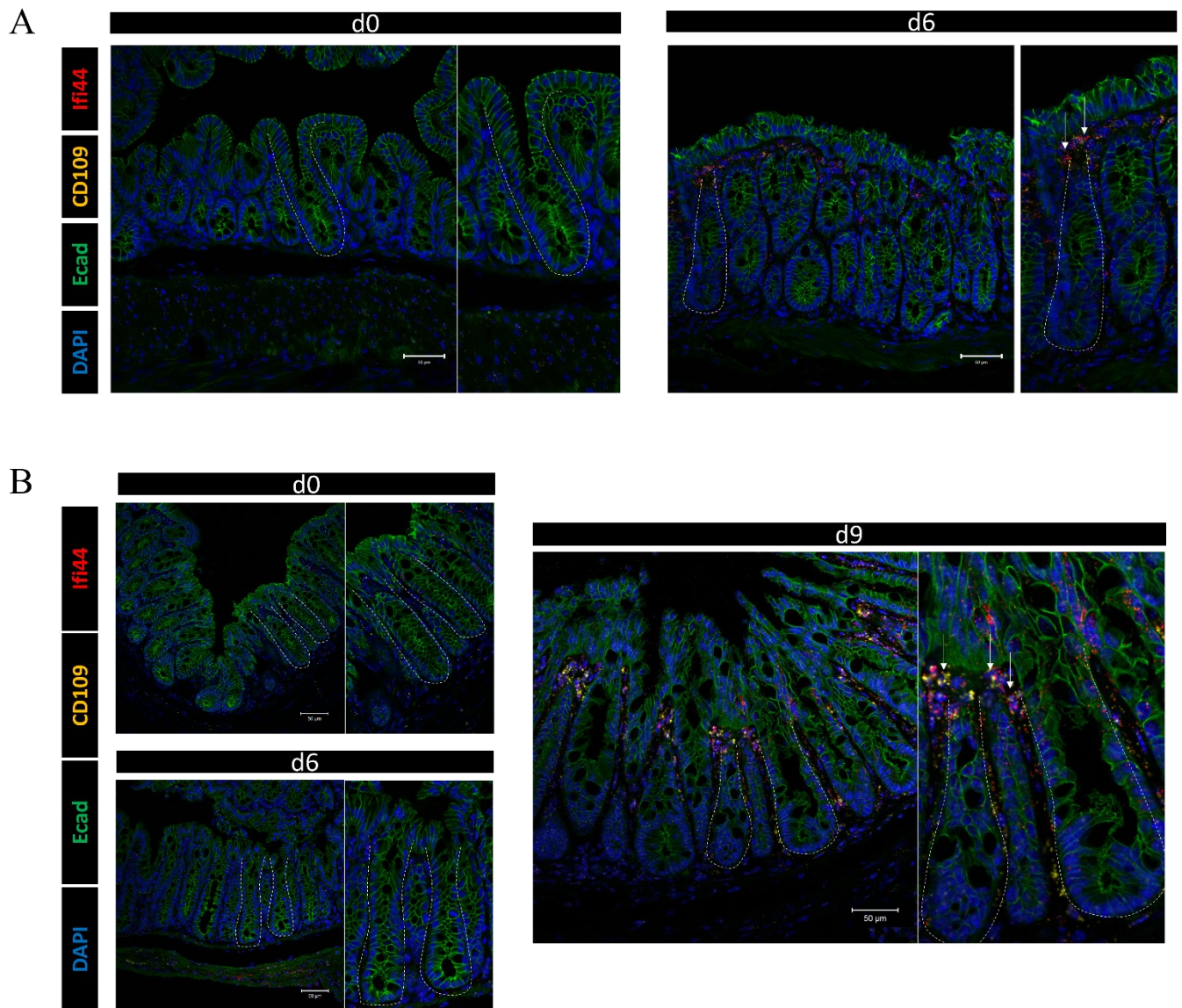


Figure 2. Fluorescent *in situ* hybridization (FISH) reveals expression of *Cd109* and *Ifi44* at early timepoints p.i. localized at the top of intestinal crypts. FFPE sections of colonic tissue were stained for *Ifi44* (red), *Cd109* (yellow), E-cadherin (green), DAPI (blue). **(A)** Sections were obtained from DAT^{tdTomato}, B6.129 mixed background mice at d0 and d6 p.i. n = 3 per timepoint. **(B)** Sections were obtained from C3H/Ouj.B6 mice at d0, d6, and d9 p.i. Crypts highlighted in insets are labelled in white, arrows indicate co-expressed *Cd109* and *Ifi44*. Scale bar = 50 μm. n = 3 per timepoint.

Next, we sought to determine if the IAF population is indeed distinct and novel from the previously characterized populations of telocytes, trophocytes, fibroblasts, and myofibroblasts through co-staining panels with FISH assays. We visualized *Grem1* and *Wnt2b* as markers for trophocytes alongside *Cd109* to respectively identify these populations. Here, *Grem1* and *Wnt2b* were highly expressed at the base of the intestinal crypts and within the underlying muscularis mucosa at d0 and d9. However, *Cd109* expression was not present at d0, and at d9 was localized at the top of intestinal crypts, segregated from the trophocytes (**Figure 3A**). For telocytes, *Bmp2* was selected as a probe to mark this stromal population. *Bmp2* localized within the epithelial cells at d0 but was completely downregulated at d9. Indeed, *Bmp2* seemed to localize separate from IAFs as *Ifi44* expression appeared only at d9 at the top of intestinal crypts (**Figure 3B**). However, for telocyte identification it is generally recognized within the stromal compartment, therefore, *Bmp7* may be a better alternate probe to mark this cellular population. For myofibroblasts, *Acta2* was used as a marker. At d0 and d9 its expression is observed between crypt units as long, thin extensions. It is also important to note that *Acta2* is highly expressed in smooth muscle tissue in the muscularis mucosa, and there was a noticeable downregulation of *Acta2* in the smooth muscle during infection. Nonetheless, *Ifi44*⁺ IAFs seemed to localize separate from *Acta2* as *Ifi44* expression appeared more closely to the apex of the crypt, whereas *Acta2* localized near the middle of the crypt (**Figure 3C**). Taken these data together, we suspect that the IAF population is indeed distinct from the currently identified stromal cell populations.

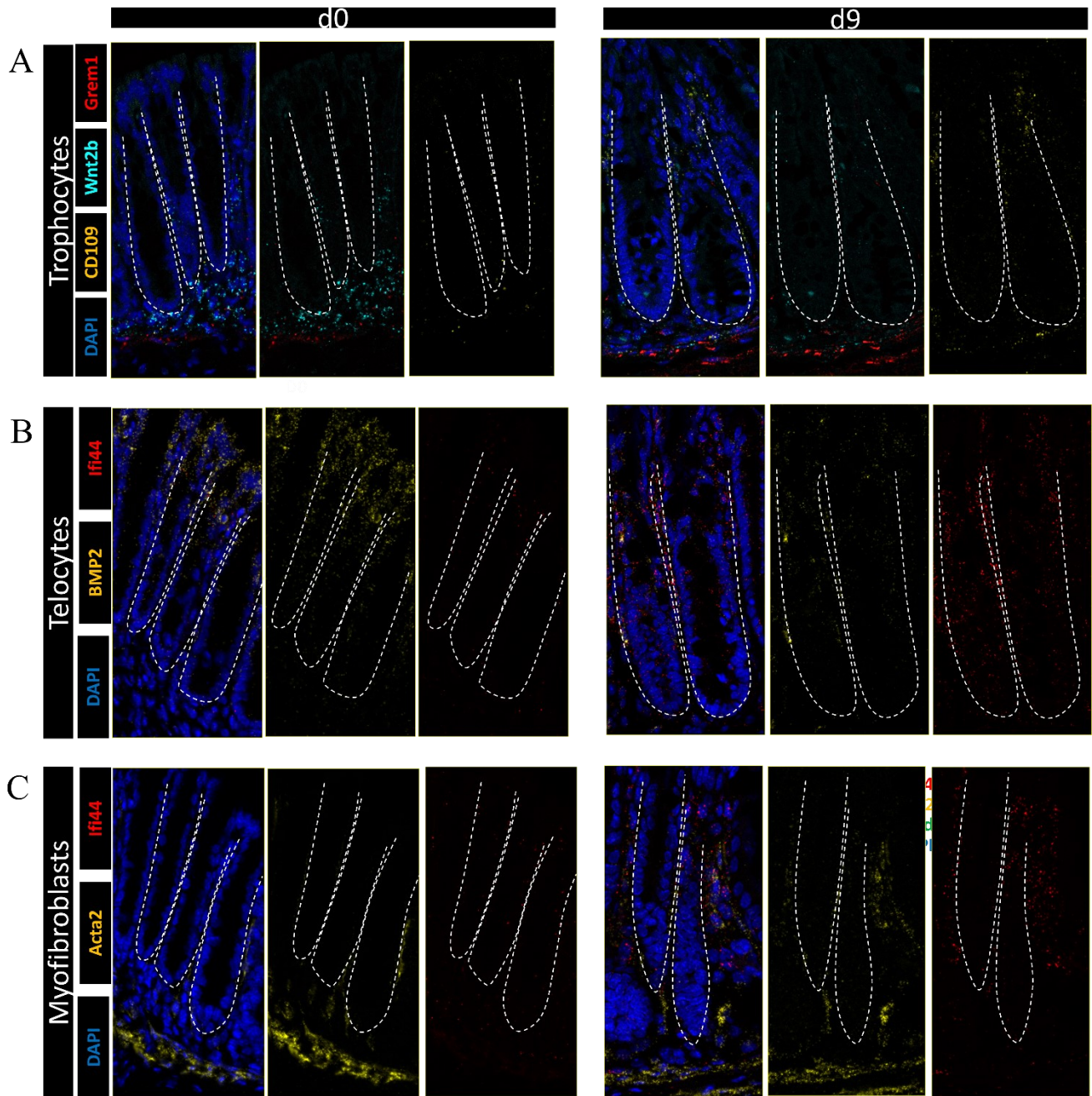


Figure 3. CD109⁺Ifi44⁺ inflammation-associated fibroblasts localize distinctly from known stromal populations, including trophocytes, telocytes, and myofibroblasts. (A) Comparison of *Cd109* (red) expression to trophocyte markers *Grem1* (yellow) and *Wnt2b* (cyan). **(B)** Comparison of *Ifi44* (red) expression and telocyte marker *Bmp2* (yellow). **(C)** Comparison of *Ifi44* (red) expression and myofibroblast marker *Acta2* (Yellow). Crypts are highlighted in insets, labelled in white. n =2 per group.

3.1.3 Treatment of primary stromal fibroblasts with IFN- γ and heat killed *C. rodentium* results in an upregulation of interferon stimulated genes and IAF markers

Given their plastic nature, we next investigated the ability for stromal cells to reprogram in culture with the appropriate inflammatory factors. We treated a heterogeneous culture of primary stromal cells with heat killed *C. rodentium*, alongside pro-inflammatory cytokines IFN- γ , TNF- α , and IL-1 β for 24 or 48 h. Specifically, upon IFN- γ and heat killed *C. rodentium* treatment, interferon stimulated genes – *Ifi44*, *Irf7*, and *Isg15* – trended upwards. However, IL-1 β and TNF- α treatment did not induce a similar upregulation (**Figure 4A-C**). Interestingly, *Cd109* was not upregulated upon any pro-inflammatory cytokine treatment nor heat killed *C. rodentium*, indicating that the *in vitro* treatments tested do not fully recapitulate the events observed *in vivo* (**Figure 4D**).

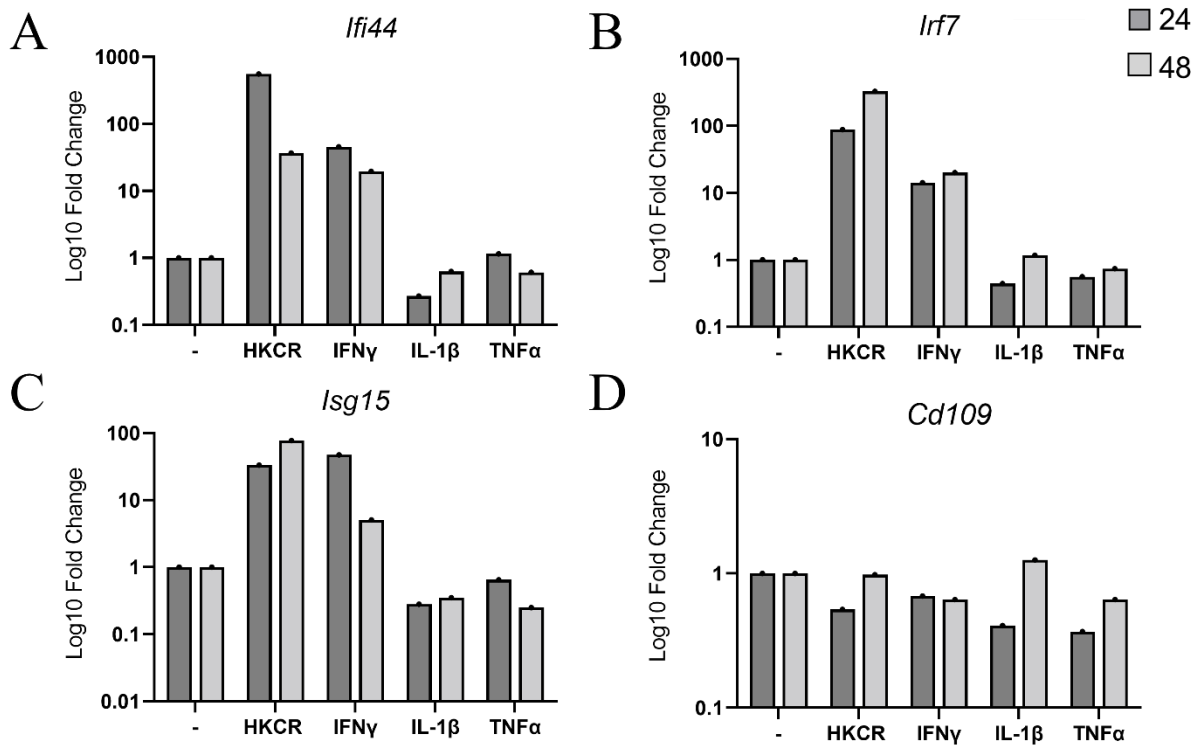


Figure 4. IFN-stimulated genes become upregulated in primary stromal cells upon IFN- γ and heat killed *C. rodentium* treatment. Primary murine stromal cells were isolated from healthy C57Bl/6 mice, grown to confluency and either left unstimulated or treated with HKCR (10⁶ CFU/mL), IFN- γ (10 ng/mL), IL-1 β (10 ng/mL), or TNF- α (20 ng/mL). Quantitative PCR (qPCR) analysis was completed to assess the relative mRNA expression levels for the following genes highly expressed in IAF subset: (A) *Ifi44*, (B) *Irf7*, (C) *Isg15*, and (D) *Cd109*. n = 1. Data points represent the mean value from technical triplicates. All qRT-PCR data was normalized to *Hprt* using the $\Delta\Delta C_t$ method.

3.1.4 Assessing the *in vivo* role of *Cd109*⁺IAFs in models of intestinal inflammation and infection.

CD109 is a multifunctional glycosylphosphatidylinositol (GPI)-anchored protein with roles in tumorigenesis and more recently described – a mediator of cutaneous inflammation (117, 118). CD109 is highly expressed in keratinocytes and certain malignant tumours; however, expression has also been reported in activated T cells, activated platelet cells, and CD34⁺ bone marrow mononuclear cells (117, 118). Amongst the stromal cell subsets, we also found *Cd109* to be a specific marker of the IAF population. As CD109 KO mice were available to us, we sought to investigate the role of CD109 during *C. rodentium* infection. CD109 WT and KO mice were infected with 2-3 x 10⁸ CFU of *C. rodentium* and sacrificed at d13 p.i. There were no significant changes in bodyweight between genotypes (**Figure 5A**). Likewise, no significant differences were observed between the bacterial shedding through CFU counts collected at d4, d8, and d12 (**Figure 5B**).

To explore if IAFs contributed to intestinal inflammation in other models, CD109 WT and KO mice were treated with 2.5% DSS supplemented-drinking water. There were no significant differences in their bodyweight loss nor colon length between genotypes, although there were non-significant trends for improved outcomes in the CD109 KO mice (less body weight loss and longer colons) (**Figure 5C-D**). Thus, although CD109 is a marker of IAFs and is involved in inflammation in other models, this preliminary information suggests it does not play a major role in intestinal *C. rodentium* infection or DSS mediated inflammation.

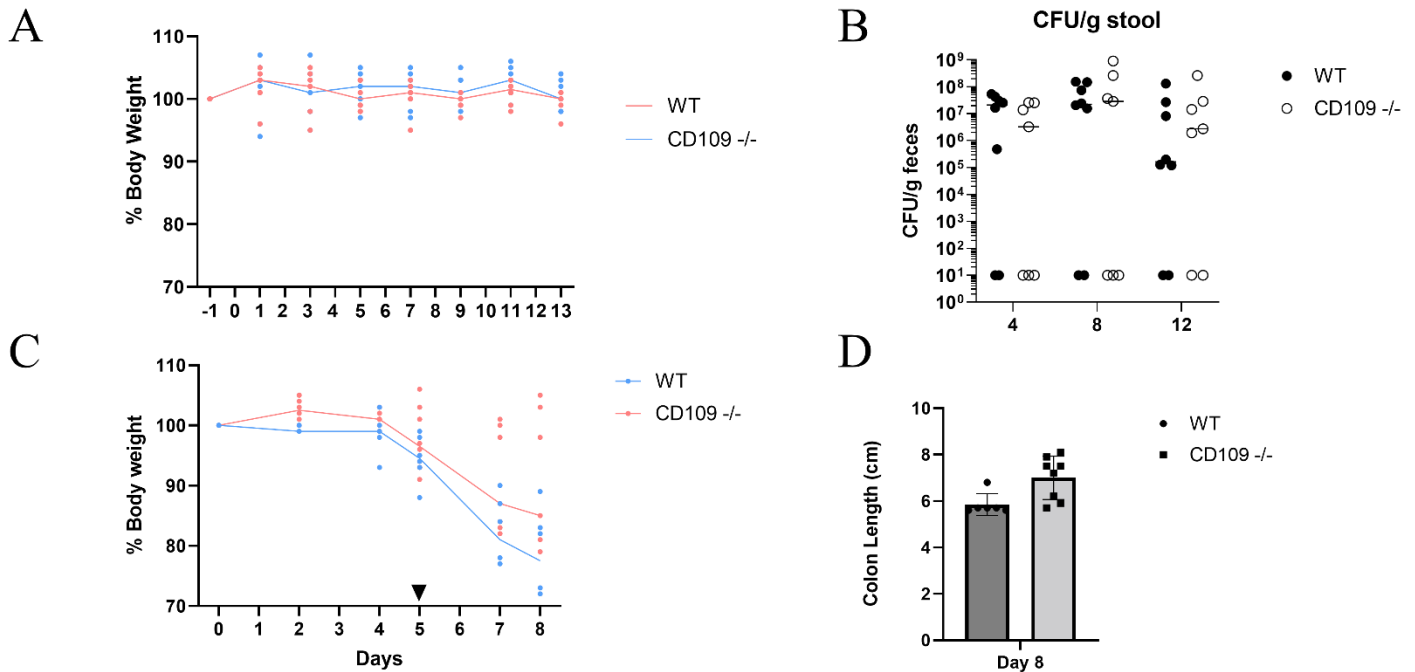


Figure 5. *Cd109* WT and KO mice do not show significant differences during *C. rodentium* infection or DSS mediated colitis. (A) Mice were infected with $2-3 \times 10^8$ CFU of *C. rodentium* and sacrificed at d13. Body weights were measured every 2 days. (B) Faecal burden assessed at d4, d8, d12 p.i. in WT; n = 8 and KO; n= 7. (C) Mice were treated with 2.5% DSS for 5 days, then transferred to normal drinking water, then sacrificed on d8. Body weights were measured every 2 days. (D) Upon sacrifice, the colon length was measured. No significance detected between groups by unpaired T-test.

3.2 Aim 2. Determine the ability of stromal cell secreted factors to mediate intestinal epithelial phenotype in inflammation and regeneration

3.2.1 Using a stromal-derived conditioned media model to understand stromal-epithelial signal mediation

We sought to investigate the ability for stromal cells to mediate epithelial regeneration through secreted factors. To do so, *ex vivo* intestinal organoid cultures were generated to produce a 3-dimensional model of the intestinal epithelium. Intestinal organoids are physiologically relevant intestinal models, derived from crypts containing Lgr5+ ISCs. When provided with essential growth factors, Lgr5+ ISCs differentiate into lineage restricted epithelial cell types and self-organize, resulting in a mature organoid with a polarized epithelium, enclosing a central lumen (12, 119). To understand stromal-epithelial signal mediation, we collected supernatant from

primary stromal cell cultures, then used this conditioned media (CM) to treat adult crypt-derived organoids.

From preliminary experiments, we observed that when organoid cultures were grown in the presence of stromal cell CM, it induced an unexpected spheroid morphology. This phenotype was unexpected as organoids grown in control conditions normally have a budding structure, generally thought to correlate with the presence of cells expressing stem cell markers (120). Notably, this spheroid morphology is reminiscent of organoids derived directly from intestinal fetal tissue (**Figure 6A**)(121, 122). Thus, we hypothesized that secreted factors within the CM may be inducing a fetal reprogramming event within the adult crypt-derived organoids. To assess what was happening on a transcriptional level, we used qPCR and observed that adult ISC markers (*Lgr5*, *Olfm4*) were downregulated and intestinal fetal markers (*Clusterin*, *Il133*, *Il1rn*) were upregulated (**Figure 6B**). Together these data indicated the possibility of a fetal reprogramming event occurring upon CM treatment.

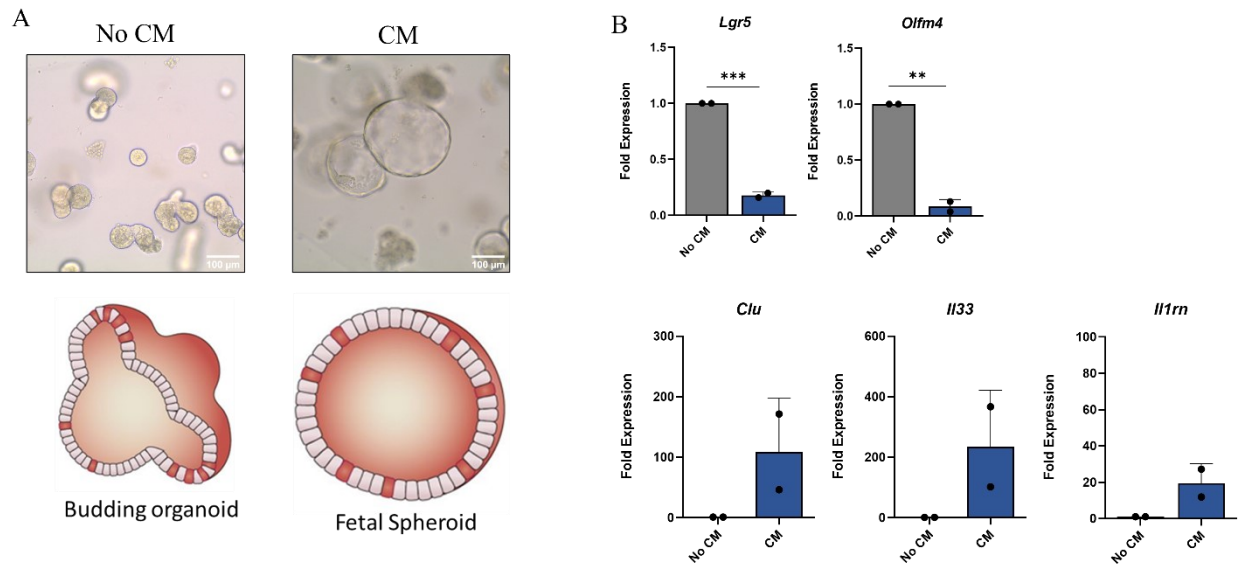


Figure 6. Stromal cell derived conditioned media (CM) induces a fetal reprogramming event in adult crypt-derived organoid cultures. Primary murine stromal cells were isolated from healthy B6 mice and grown to confluency. CM was aliquoted and incubated with freshly plated adult murine crypt-derived SI organoids. (A) Brightfield (BF) images of organoids with No CM (control) or CM. Scale bar = 100µm (B) Quantitative PCR (qPCR) analysis of adult ISC markers (*Lgr5*, *Olfm4*) and (C) fetal markers (*Clusterin*, *Il33*, *Il1rn*). Data points represent the mean value from two individual independent experiments and error bars represent SD. All qRT-PCR data was normalized to *Hprt* using the $\Delta\Delta C_t$ method. **P < 0.01, *** P < 0.001 by unpaired T-test.

3.2.2 Stromal-derived PGE2 may induce a fetal reprogramming response in the intestinal epithelium

A secreted factor within our stromal CM that we hypothesized might induce the observed fetal reprogramming event is prostaglandin-E2 (PGE2). PGE2 is a physiologically active lipid, recently shown to be involved in intestinal epithelial regeneration and to induce a fetal-like state in organoids (123). Additionally, certain stromal cells have been shown to produce PGE2 (123). To investigate this possibility, we first referred to our scRNAseq database to determine if our stromal populations express genes that encode synthesis enzymes for PGE2 production. Indeed, most stromal cells in our dataset expressed *Ptgs1/2*, which encodes the rate limiting enzyme in PGE2 production – COX-1/2. COX-1/2 converts arachidonic acid, a lipid precursor, into the prostaglandin-H2 intermediate (PGH2). These stromal cells also expressed *Ptges* which encodes the terminal synthesis enzyme, mPGES-1, converting PGH2 into PGE2 (**Figure 7A-B**) (124).

We first stimulated organoids directly with PGE2 for 48h to determine if the phenotype and gene expression patterns observed in our CM cultures could be recapitulated. Notably, while the spheroidal organoids were observed upon PGE2 stimulation (**Figure 7C**), the gene signature was only partially recapitulated by an upregulation in the fetal markers and no downregulation in the ISC markers was observed (**Figure 7D**).

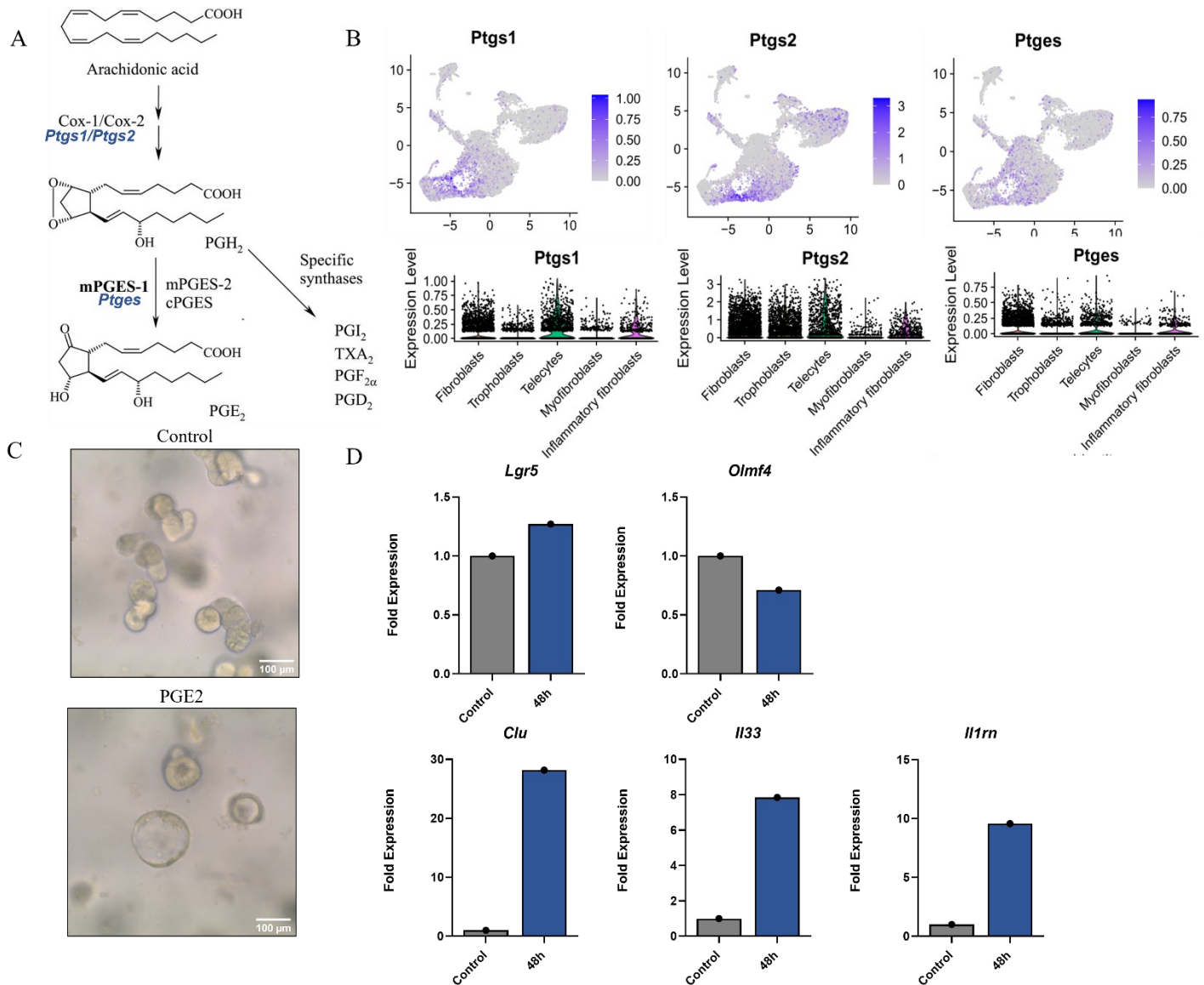


Figure 7. Prostaglandin-E2 (PGE₂) stimulation partially recapitulates fetal reprogramming in intestinal epithelial organoids. (A) Major enzymes within the PGE₂ synthesis pathway, adapted from (124). (B) Feature plots and corresponding violin plots depicting relative expression of *Ptgs1*, *Ptgs2*, and *Ptges* amongst the stromal populations detected via scRNAseq. (C) Brightfield images of adult crypt-derived organoids that were left unstimulated or stimulated with 10 μM of PGE₂ for 48 h, refreshing every 24 h. Scale bar = 100 μm. n = 1 per treatment group. (D) Quantitative PCR (qPCR) analysis of adult ISC markers (*Lgr5*, *Olfm4*) and fetal markers (*Clusterin*, *Il33*, *Il1rn*). Data points represent the mean value from one individual independent experiment. All qRT-PCR data was normalized to *Hprt* using the $\Delta\Delta C_t$ method.

To investigate this further, we isolated primary stromal cells from whole body mPGES-1 KO and WT littermate control mice. Additionally, we treated the mPGES-1 WT stromal cells with indomethacin (IND) – a drug that is a direct inhibitor of COX1/2. The stromal cells were grown to confluency; following, CM was collected and incubated with fresh crypt-derived organoids. We observed that stromal cell CM derived from WT mPGES-1 mice led to significant spheroid

induction, with up to 40% spheroids induced per well, and distinct upregulation of fetal gene expression (**Figure 8A-C**). Conversely, while CM derived from WT mPGES-1 stromal cells treated with IND resulted in significant spheroid induction, its upregulation was not nearly as stark as WT CM with only 10% spheroids induced per well, and no significant fetal gene upregulation. Similarly, CM from KO mPGES-1 stromal cells had greatly reduced spheroid formation and fetal gene expression. Together, these data validate that PGE2 is partially responsible for the fetal reprogramming response induced by stromal cell CM; however, it may not be acting alone.

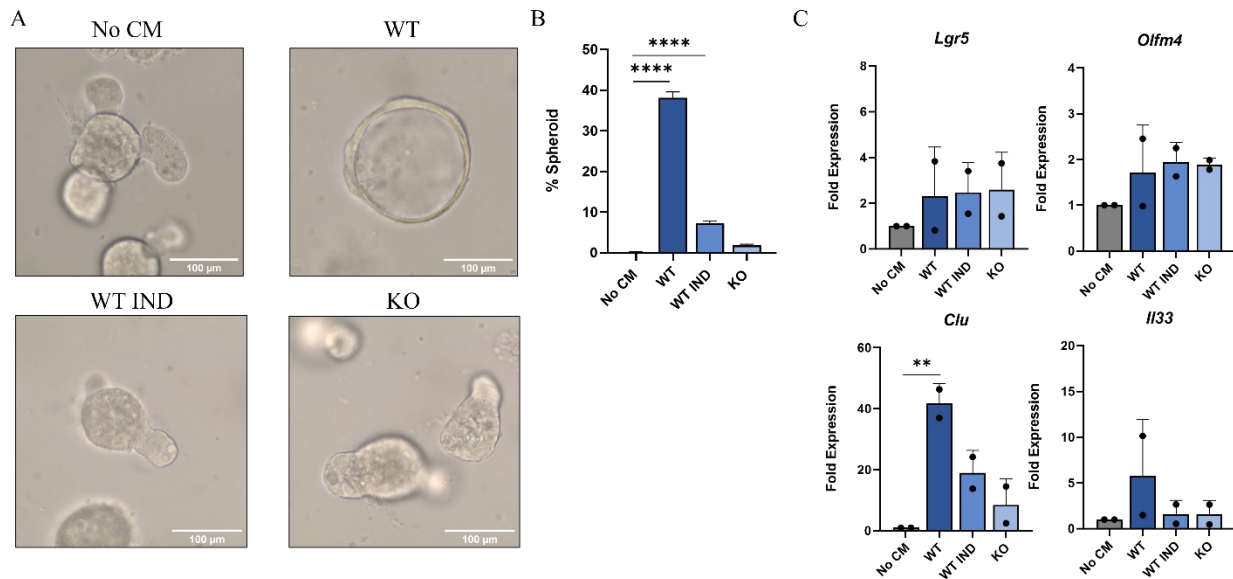


Figure 8. Downregulation of Prostaglandin-E2 (PGE2) in culture reverts fetal organoid phenotype. (A) Brightfield images of organoids incubated with no CM control, CM derived from mPGES-1 WT mice with or without indomethacin stimulation, and CM from mPGES-1 KO mice. (B) Quantification for spheroid counts per condition. Two wells per 24 well plate were counted per condition. (n = 2 biological replicates). (C) Quantitative PCR (qPCR) analysis of adult ISC markers (*Lgr5*, *Olfm4*) and fetal markers (*Clusterin*, *Il33*). Data points represent the mean value from two individual independent experiments and error bars represent SD. All qRT-PCR data was normalized to *Hprt* using the $\Delta\Delta C_t$ method. **P < 0.01, **** P < 0.0001 by one-way ANOVA and Dunnett's post-test with No CM group set as control.

3.2.3 Investigating the role of PGE2 on intestinal epithelial wound healing in vivo

When the intestine is subjected to severe damage, *Lgr5*⁺ ISCs become ablated (17). The subsequent regeneration mechanisms are dependent upon re-initiation of early developmental programs through DASC populations, which are generally quiescent under homeostasis. These quiescent DASCs will repopulate the *Lgr5*⁺ ablated crypts by reverting to a more primitive state

through fetal reprogramming events; thereby, upregulating fetal-like transcriptional programs, driving uniform proliferation, tissue remodeling, and restoring homeostasis (120). As previously mentioned, there are several subpopulations of DASCs, including cells with high expression of *Hopx*, *Bmi1*, *Tert*, *Lrig1*, or *Clu*. (21–25). Thus, we sought to investigate if stromal-derived PGE2 could directly influence recovery mechanisms, specifically in Clu⁺ DASCs.

Clu⁺ cells are one of several DASC populations that have been shown to repopulate the entire ISC crypt following severe damage like irradiation and colitis (25). To understand the intersection of Clu and PGE2, we used a lineage tracing model in Clu^{tdTomato} reporter mice crossed with mPGES-1 KO and WT littermate controls. The Clu^{tdTomato} mice were previously generated by breeding CluCreERT2 and Rosa Lox-Stop-Lox tdTomato mice, providing a system where, the labeling of Clu⁺ cells is inducible through Tamoxifen (TAM) injection (**Figure 9A**). The mice were subjected to 2.5% DSS – targeting the colon, to model severe colitis. An additional cohort of mice were subjected to 12 Gy of irradiation to investigate repair of damaged crypts in the small intestine in a model where inflammation is not the primary insult.

In the colitis model, mice were administered 2.5% DSS for 5 days, followed by a TAM injection on d6, and sacrificed on d9. Through IHC staining, we observed that post DSS treatment, mPGES-1 KO mice demonstrated a distinct downregulation of Clu^{tdTomato} cells in recovering epithelial wounds compared to mPGES-1 Het (**Figure 9B**). Alternatively, in the irradiation model, mice were first injected with TAM on d1, irradiated on d2, and sacrificed on d7. Upon IF staining, tdTomato expression was quantified based on the total labeling of intestinal crypts. Between Clu^{tdTomato} mPGES-1 WT, Het, and KO mice, there was no detectable difference in the number of tdTomato⁺ cells from the Clu⁺ lineage (**Figure 9C**). Together these data indicate that PGE2 may not influence Clu⁺ DASCs and their progeny following irradiation damage in the small intestine. However, PGE2 may influence migration of Clu⁺ DASCs during epithelial wound repair in the colon following DSS treatment.

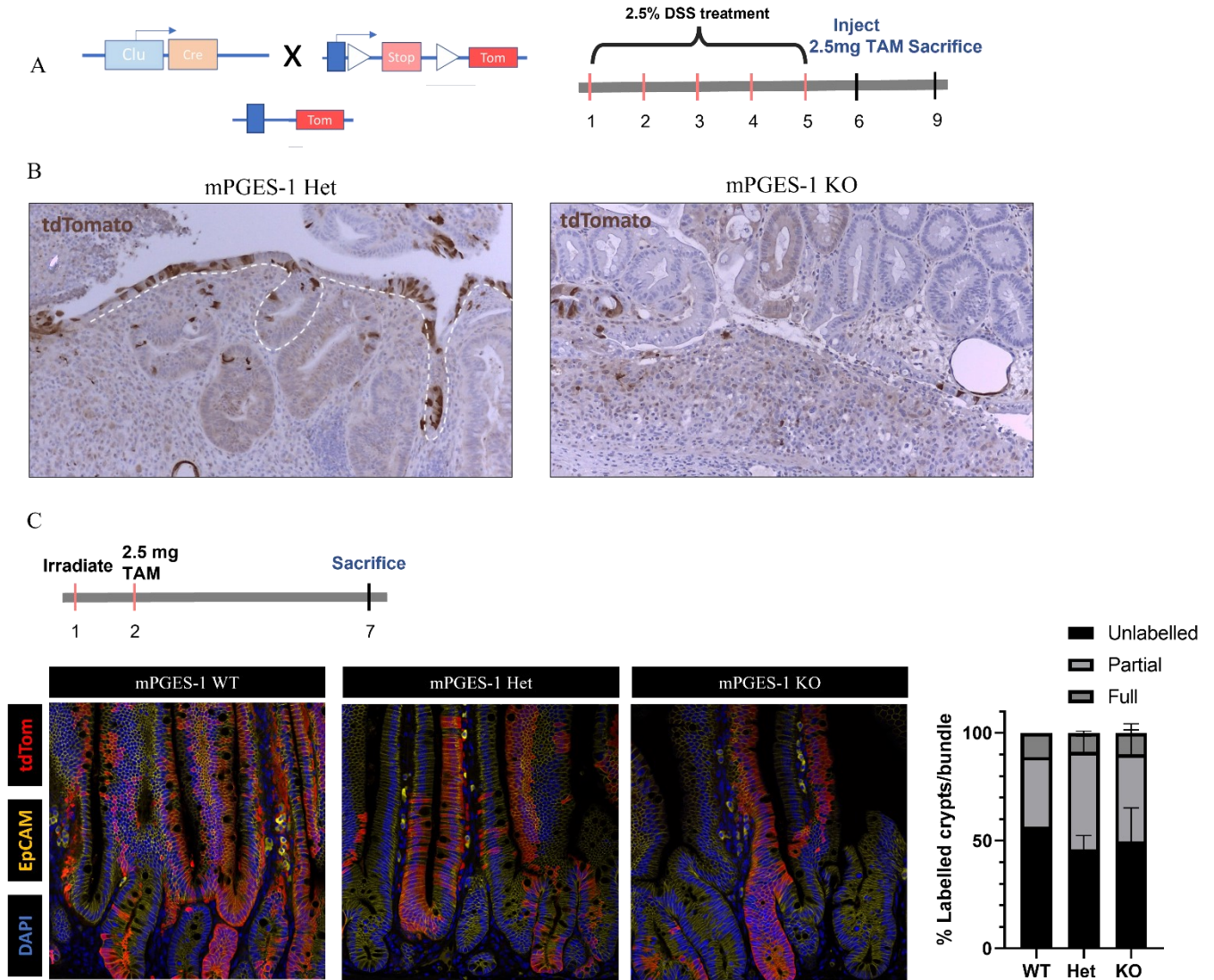


Figure 9. Downregulation of PGE2 may affect the migration and wound recovery of the colonic epithelium post DSS treatment. (A) Schematic representation of Tamoxifen-induced Cre activity in $Clu^{tdTomato}$; mPGES-1 WT, Het and KO mice. 2.5% DSS was added to drinking water for 5 days, then switched back to normal water. Mice were injected with 2.5 mg of TAM on d6 and sacrificed on d9. (B) IHC staining of colonic tissue for tdTomato. Het; n = 2 and KO; n = 2, crypts outlined in white dashed line. (C) IF staining for lineage trace of $Clu^{tdTomato}$ cells in mPGES-1 WT, Het, and KO mice. To quantify, 3-5 cross-sections of the SI were counted, whereby each crypt was denoted as unlabelled, partial, or fully labelled depending on the level of epithelial tdTomato staining, then plotted as a % labeled crypt/cross section. WT; n = 1, Het; n = 2 and KO; n = 3. No significance detected between genotypes by two-way ANOVA.

CHAPTER 4: DISCUSSION

4.1 Aim 1 – Analyzing the response of the intestinal stromal cell compartment following infection with *C. rodentium*

The intestinal stromal compartment is a highly heterogeneous and plastic population of cells, our understanding of its composition is continually evolving. Characterization of the distinct cell types within the intestinal stromal compartment has remained a challenge until recent years (11). With the advent and accessibility of scRNAseq, Cre-driver mouse models, organoid co-cultures, and fine-resolution microscopy, there has been an increase of studies resolving the stromal composition and cellular sources for many secreted factors that support the intestinal crypt architecture (89). Notably, our understanding of the stromal compartment under homeostatic conditions has been significantly refined in the past decade. Subsequently, many groups are now interested in how the stromal compartment is affected under inflammatory conditions. Two independent studies demonstrated that during severe intestinal inflammation, as seen in IBD, the stromal compartment undergoes a remodeling event where inflammatory-associated stromal subsets are induced and exacerbate inflammatory conditions (80, 103). However, few studies have discussed the effect of intestinal infection on stromal compartment remodeling.

Here, we used scRNAseq to better understand the extent of cellular heterogeneity in the stromal compartment during a mouse enteric infection model. We have demonstrated that upon *C. rodentium* infection, there is an emergence of a novel stromal population that we have dubbed inflammatory-associated fibroblasts (IAFs). Marked by *Cd109⁺Ifi44⁺* expression, these IAFs are undetectable prior to infection; however, at early timepoints of infection, they are visible by FISH at the tops of colonic crypts (**Figure 2A, C**). We suspect they have immunomodulatory functions as the GO terms associated with this population correspond with roles like T cell activation and antigen processing and presentation (**Figure 1D**). While we have confirmed the presence of the IAF population histologically at d6 and d9, we must still confirm if they are no longer present at later timepoints like d13 – in correspondence with the scRNAseq data.

There are still many open questions about their function and mechanism of action that remain to be answered. Notably, what early immune response cues may be triggering the transient

emergence of the IAF subset, where the IAF population is originating from, and what downstream interactions are occurring with immune cells to facilitate or exacerbate inflammation?

We speculate that early signals in the innate immune response to *C. rodentium* infection may be inducing the emergence of IAFs. *In vitro* we stimulated primary stromal cells with HKCR and pro-inflammatory cytokines: IFN- γ , TNF- α , and IL-1 β . Notably, only HKCR and IFN- γ treatment resulted in upregulation of ISG-associated IAF genes. Indeed, with reference to our scRNAseq dataset, we observe that IAFs express multiple IFN receptors, including IFN- γ receptors *Ifngr1* and *Ifngr2*; however, their expression is not specific to the IAF population, and multiple other stromal populations also express these receptors (data not shown). It is also important to note that in the primary stromal culture, HKCR and IFN- γ treatment did not lead to an upregulation of other IAF genes like *Cd109* (**Figure 4**). Thus, we speculate that early *C. rodentium* infection induces a cocktail of secreted cytokines which together may mediate the transient appearance of IAFs. With respect to which innate immune cells are involved in early infection; we investigated an additional scRNAseq dataset of immune cells obtained in parallel to the stromal cells presented in this study. In the immune dataset, we observed a significant increase in granulocyte and monocyte populations d6 p.i. in coincidence with the transient emergence of IAFs (data not shown). We hypothesize that cytokines secreted by these immune cells may trigger remodeling, leading to the emergence of IAFs. For instance, granulocytes and monocytes will secrete IL-1 β , IL-6, and IL-12 during early infection (126).

We are also interested in understanding the cellular source of the IAF population. A possible line of thought is that IAFs may arise from remodeling of myofibroblasts within the stromal compartment. Our previous work has shown that myofibroblast and smooth muscle markers *Acta2* and *Myh11* become significantly downregulated in response to *C. rodentium* infection (data not shown). We speculated that the decrease in myofibroblast markers were indicative of a stromal remodeling event and were giving rise to the transient IAF population. Notably this phenomenon was also observed in a murine breast cancer tumour model. Here, Grauel et al. were interested in the heterogeneity of cancer-associated fibroblasts (CAFs) in the tumour microenvironment, and remodeling that occurs within the CAF subsets upon TGF- β blockade (127). Through scRNAseq, they determined that anti-TGF- β treatment of 4T1 breast cancer tumours resulted in significant reduction of cancer-associated myofibroblasts (myCAFs)

accompanied by the appearance of a transcriptionally unique population of CAFs – dubbed interferon-licensed CAFs (ilCAFs) (127). They suspected that ilCAFs may arise from the reprogramming of existing myCAFs in response to anti-TGF- β treatment. Strikingly similar to our observations, the DEGs associated with the ilCAF population involved several interferon-stimulated genes (ISGs) such as *Ifi47* and *Ifitm1*. Likewise, ilCAFs were reported to have immunomodulatory properties, with GO terms like MHC class I antigen processing and presentation and immunoregulatory interactions (127). Together, these results help support our own myofibroblast-IAF remodeling event within the *C. rodentium* infection model. It is interesting to note that CD109 itself is reported as a negative regulator of TGF- β signaling in keratinocytes (118). Likewise, *C. rodentium* infection itself induces a decrease in TGF- β receptor I and II, with downstream decreases in SMAD 2, 3, 4 and 7 in the mouse colon. It is suspected that decrease in TGF- β signaling promotes inflammation and contributes to disease pathogenesis (128). Taken together, these lines of thought may indicate a plausible mechanism between a decrease in TGF- β signaling, inducing a myofibroblast-IAF remodeling event. However, this hypothesis will require further validation.

With respect to our myofibroblast-to-IAF remodeling hypothesis, our collaborators completed pseudotime analysis to trace the population to which the IAFs were most closely related. To our surprise, the IAFs were most closely related to the general fibroblast population, rather than myofibroblasts themselves (data not shown). Interestingly, Grauel et al also noted this discrepancy in their pseudotime analysis, but still suspected that ilCAFs were arising from remodeling of myofibroblasts. Therefore, additional validation is still needed to investigate these open questions. Lineage tracing of general fibroblast populations can be completed through inducible Cre-LoxP reporter systems. Here, we can complete RNAscope with IAF markers to determine if they colocalize with fibroblast progeny. There is also a possibility that the downregulation in *Acta2* and *Myh11* expression we observed in our qPCR analysis of whole colonic tissue is due to a decrease of smooth muscle in response to *C. rodentium* infection, as this phenomenon is observable in the RNAscope staining in **Figure 3E**.

Speculating the downstream interactions between IAFs and immune cells, we observe that GO terms related to T cell activation and antigen processing and presentation are upregulated in the IAF population. The capacity for intestinal stromal cells to interact with lymphocytes through

MHC class I expression has been previously described (85). Indeed, these IAFs may be interacting with CD8⁺ T cells through MHC class I presentation. However, more recently, certain stromal cell populations like myofibroblasts have been shown to constitutively express MHC class II *in vivo* (129). Likewise, several groups have identified that *in vitro* primary human colonic myofibroblasts were capable of stimulating allogeneic CD4⁺ T cell proliferation as a non-professional antigen presenting cell (85, 129). With respect to *C. rodentium* infection, CD4⁺ T cells are a prominent component of the humoral response to infection, and are essential in pathogen clearance (109). Therefore, it is possible that IAFs may be contributing to their recruitment to the site of infection. More work is needed to elucidate the specific chemokines expressed by the IAF population, additionally analysis of the ligand-receptor interactions between stromal and T cells may be beneficial to better understand the nature of their communication.

It is also important to mention the limitations of this study. Use of a whole-body knockout of CD109 has its disadvantages, as aforementioned, CD109 is expressed in many different cell types including keratinocytes. Thus, there is a possibility of other impacted cellular systems which could influence our results. Additionally, although CD109 is highly upregulated in the IAF population, other candidate markers are worth investigating, for instance, *Neto2* that may be more limited to the IAF stromal population. However, given the heterogeneous and plastic nature of stromal cells, there is always the risk of certain overlap between molecular markers. Another mouse model we could pursue is a stromal specific IFN-receptor knockout to determine how IFN-signaling directly affects the transient emergence of the IAF population and their potential function. Currently, we have *Colla2^{CreERT}; Ifngr fl/fl* mice that could be used to investigate this stromal specific-IFN- γ KO.

4.2 Aim 2.1 – Modeling stromal-epithelial signaling in an *ex vivo* setting

A key feature of stromal cells is their dynamic communication with adjacent epithelium and their contribution to maintaining the epithelial barrier. To better understand the mechanisms of signaling, we developed a reductionist model of stromal-epithelial communication, in which stromal CM was cultured with crypt-derived organoids. Here, we observed that the addition of CM resulted in an unexpected spheroid phenotype in adult-crypt derived organoids rather than budding organoids, as seen in control conditions (**Figure 6**). As aforementioned the spheroid phenotype is reminiscent of organoids derived from fetal tissue (121, 122). Given these observations, we

suspected that secreted factors within the stromal-derived CM may be inducing a fetal reprogramming event on the crypt-derived organoids.

A recently described candidate responsible for inducing such events is PGE2 (120, 123). Roulis et al demonstrated that fibroblast-induced fetal reprogramming in crypt-derived organoids is dependent on the release of PGE2. Specifically, they identified a rare subset of pericryptal fibroblasts which mediated the release of PGE2 acting on the *Ptger4* receptor of intestinal epithelial cells (123). To observe the effects of soluble mediators produced by fibroblasts on the intestinal epithelium, they used an organoid co-culture model in which primary intestinal fibroblasts were plated directly underneath fresh crypts. Similar to our stromal-derived CM cultures, their co-culture conditions consistently produced spheroids. Additionally, RNA-seq analysis revealed that DASCs were a major cell type contributing to the spheroid composition with notable increase in *Clu* and *Il1rn* expression, aligning with our current findings (123).

While the stromal-epithelial CM is beneficial as a reductionist model of communication between these two cellular populations, there are several limitations. Notably, in an organoid culture, there is no recapitulation of the gradient of signaling molecules along a crypt-villus axis that is a prominent feature *in vivo*. As aforementioned in the introduction, specific localization of Wnt and Bmp secretion contributes to the patterning of the crypt-villus architecture. Additionally, in our culture system we modeled the stromal-epithelial communication in a unidirectional manner, whereas this interaction occurs in a bidirectional manner. In the future we would suggest a co-culture system with stromal cells grown below intestinal organoids.

It is also important to note that our stromal cultures were a heterogeneous mix of subsets as we did not discriminate or sort for different cell types. As a result, we did not distinguish the specific cell type responsible for PGE2 production, or if several populations contributed to PGE2 synthesis. Given our scRNAseq data, we observed that many subsets do indeed express genes necessary to encode for PGE2-synthesis enzymes. Thus, in the future we would like to further investigate this distinction. We would also like to evaluate the level of PGE2 within our CM to fully validate the presence and function of this bioactive lipid.

4.3 Aim 2.2 – Modeling the effect of stromal-derived PGE2 on intestinal epithelial regeneration *in vivo*

Given our findings from the *ex vivo* data, we sought to better understand the effect of PGE2-mediated fetal reprogramming and epithelial repair in an *in vivo* context. As aforementioned, fetal reprogramming is a phenomenon that occurs after severe epithelial damage. Lgr5⁺ ISCs become ablated, so quiescent DASCs or certain progenitors must dedifferentiate to a more primitive state to repair the tissue. They will upregulate transcription of fetal genes that are normally associated with embryonic gut development (ex. *Ly6a*, *Clu*, *Anxa1*, *Il-33*). This temporary reversion to a fetal-like state will facilitate uniform epithelial proliferation and remodel the damaged tissue (120). Notably, fetal reprogramming requires the activity of Yes-associated protein (YAP), an important effector in the Hippo pathway, active in tissue regeneration and organogenesis (130, 131).

We speculated that stromal-derived PGE2 was mediating the induction of Clu⁺ DASC fetal reprogramming in response to severe intestinal damage, given that *Clu* is a crucial gene in the fetal reprogramming signature (130). We therefore employed the use of Clu^{tdTomato}; mPGES-1 KO mice and littermate controls, providing a lineage trace for Clu⁺ DASCs and cell progeny, and their response to downregulated PGE2 production. Interestingly, we observed that the level of PGE2 does not alter the expansion of Clu⁺ epithelial cells in the SI following irradiation damage, but it may influence the migration of Clu⁺ cells within the colon following DSS treatment (**Figure 9C**). Here, we observed that in mPGES-1 Het mice, tdTomato⁺ cells emanated from recovering crypts and migrated over the DSS-mediated wound bed. Conversely, in mPGES-1 KO mice, there was very little staining of tdTomato⁺ cells.

In comparison with available literature, others have observed a more pronounced effect of PGE2 on the mediation of DASC expansion. Specifically, Roulis et al demonstrated that *in vivo*, pericryptal fibroblast-derived PGE2 caused significant expansion of Sca-1⁺ DASCs in the mediation of tumorigenesis. They also observed that this event occurred in a YAP dependent manner (123). However, one of the biggest differences between our models is the means of downregulating PGE2 production *in vivo*. While Roulis et al knocked out a major PGE2 receptor EP4 (encoded by *Ptger4*) we knocked out mPGES-1 synthesis enzyme. A limitation we must consider is that in addition to mPGES-1, there are several other pathways capable of converting PGH2 intermediate into PGE2. While mPGES-1 is known to play a role in human disease by

promoting inflammation, pain, and fever, additional enzymes such as cPGES and mPGES-2 are shown to be constitutively expressed during homeostasis (124). Thus, mPGES-1 may downregulate PGE2 levels but does not necessarily constitute a complete ablation of its production. Moving forward, deleting *Ptger4* within Clu^+ cells would be a more specific model to target PGE2 signaling. Another important consideration is that in addition to stromal-derived PGE2, immune cells are also reported as strong producers of PGE2 in an inflammatory context within the intestinal environment (125). While we have demonstrated that stromal cells are a likely source of PGE2 through *ex vivo* CM modeling, a future direction would be to decipher the contribution of stromal versus immune secretion of PGE2 through stromal specific KOs of PGE2 synthesis enzymes.

Additional future experiments we would like to pursue is a time course investigating the emanation of Clu^+ cells on the epithelial wound bed and when these events occur in regeneration. Interestingly, Miyoshi et al have observed a similar repair mechanism, where sterile colonic biopsy resulted in increased numbers of *Ptgs2*⁺ mesenchymal cells that produce PGE2 to promote formation of wound associated epithelial (WAE) cells (132). Here, WAE cells emanate from surviving crypts adjacent to the damaged epithelium and are dependent on stromal-derived PGE2 for their migration (132).

CHAPTER 5: CONCLUSION

Emerging data within the past decade has significantly refined our understanding of the heterogeneity, function, and localization of intestinal stromal cell subsets under homeostatic conditions. We increasingly understand that stromal cells are not solely passive structural cells, and they act as critical sources of signaling factors contributing to the intestinal architecture, ISC proliferation, and epithelial lineage differentiation. However, only recently have investigators turned their attention towards the role of stromal cells in intestinal inflammation and infection. Our work provides some insight into the intestinal stromal remodeling that occurs specifically under enteric infection, as well as a role of stromal-derived PGE2 in the response to epithelial wound healing.

In aim 1, through *in vivo* *C. rodentium* infection models, we demonstrated the transient emergence of a potentially novel stromal cell subset that we have dubbed inflammatory-associated fibroblasts (IAF). Marked by *Cd109⁺Ifi44⁺*, we have validated the emergence of IAFs histologically. While we are still in the early stages of elucidating their function, we believe they may contribute to host-defense and immunomodulation against *C. rodentium*, and we speculate if this population is also involved in other infectious or inflammatory disorders. In aim 2, we demonstrated a reductionist stromal-organoid conditioned media culture system, representing a unidirectional stromal-epithelial communication. Through this system, we were able to identify prostaglandin-E2 (PGE2) as a driver of fetal reprogramming *ex vivo* and provided preliminary results of PGE2 as a mediator of epithelial wound healing in an *in vivo* DSS model.

In general, these studies help contribute to the greater understanding of stromal cell heterogeneity, and their role in responding to infectious agents and inflammatory damage of the intestinal tract.

References

1. Reed, K. K., and R. Wickham. 2009. Review of the Gastrointestinal Tract: From Macro to Micro. *Semin. Oncol. Nurs.* 25: 3–14.
2. Barker, N. 2013. Adult intestinal stem cells: critical drivers of epithelial homeostasis and regeneration. *Nat. Rev. Mol. Cell Biol.* 2013 151 15: 19–33.
3. Roulis, M., and R. A. Flavell. 2016. Fibroblasts and myofibroblasts of the intestinal lamina propria in physiology and disease. *Differentiation* 92: 116–131.
4. Greenwood-Van Meerveld, B., A. C. Johnson, and D. Grundy. 2017. Gastrointestinal physiology and function. *Handb. Exp. Pharmacol.* 239.
5. Campell, Jacob; Berry, James; Liang, Y. 2020. *Anatomy and Physiology of the Small Intestine*,.
6. Szmulowicz, U. M., and T. L. Hull. 2011. Colonic Physiology. *ASCRS Textb. Colon Rectal Surg.* 23–39.
7. Gehart, H., and H. Clevers. 2019. Tales from the crypt: new insights into intestinal stem cells. *Nat. Rev. Gastroenterol. Hepatol.* 16: 19–34.
8. Clevers, H. 2013. The Intestinal Crypt, A Prototype Stem Cell Compartment. *Cell* 154: 274–284.
9. Bonis, V., C. Rossell, and H. Gehart. 2021. The Intestinal Epithelium – Fluid Fate and Rigid Structure From Crypt Bottom to Villus Tip. *Front. Cell Dev. Biol.* 9.
10. Wood, J. D. 2004. Enteric Nervous System. *Encycl. Gastroenterol.* 701–706.
11. McCarthy, N., J. Kraiczy, and R. A. Shivdasani. 2020. Cellular and molecular architecture of the intestinal stem cell niche. *Nat. Cell Biol.* 22: 1033–1041.
12. Sato, T., R. G. Vries, H. J. Snippert, M. Van De Wetering, N. Barker, D. E. Stange, J. H. Van Es, A. Abo, P. Kujala, P. J. Peters, and H. Clevers. 2009. Single Lgr5 stem cells build crypt-villus structures in vitro without a mesenchymal niche. *Nat.* 2009 4597244 459: 262–265.
13. Cheng, H., and C. P. Leblond. 1974. Origin, differentiation and renewal of the four main epithelial cell types in the mouse small intestine V. Unitarian theory of the origin of the four epithelial cell types. *Am. J. Anat.* 141: 537–561.
14. Barker, N., J. H. Van Es, J. Kuipers, P. Kujala, M. Van Den Born, M. Cozijnsen, A. Haegebarth, J. Korving, H. Begthel, P. J. Peters, and H. Clevers. 2007. Identification of stem cells in small intestine and colon by marker gene Lgr5. *Nat.* 2007 4497165 449: 1003–1007.
15. Beumer, J., and H. Clevers. 2021. Cell fate specification and differentiation in the adult mammalian intestine. *Nat. Rev. Mol. Cell Biol.* 22: 39–53.
16. Van Der Flier, L. G., and H. Clevers. 2009. Stem cells, self-renewal, and differentiation in the intestinal epithelium. *Annu. Rev. Physiol.* 71: 241–260.
17. Bankaitis, E. D., A. Ha, C. J. Kuo, and S. T. Magness. 2018. Reserve Stem Cells in Intestinal Homeostasis and Injury. *Gastroenterology* 155: 1348–1361.
18. Rees, W. D., R. Tandun, E. Yau, N. C. Zachos, and T. S. Steiner. 2020. Regenerative Intestinal Stem Cells Induced by Acute and Chronic Injury: The Saving Grace of the Epithelium? *Front. Cell Dev. Biol.* 8: 1333.
19. Tian, H., B. Biels, S. Warming, K. G. Leong, L. Rangell, O. D. Klein, and F. J. De Sauvage. 2012. A reserve

- stem cell population in small intestine renders Lgr5-positive cells dispensable. *Nature* .
20. Beumer, J., and H. Clevers. 2016. Regulation and plasticity of intestinal stem cells during homeostasis and regeneration. *Development* 143: 3639–3649.
 21. Takeda, N., R. Jain, M. R. LeBoeuf, Q. Wang, M. M. Lu, and J. A. Epstein. 2011. Interconversion between intestinal stem cell populations in distinct niches. *Science* 334: 1420–1424.
 22. Sangiorgi, E., and M. R. Capecchi. 2008. Bmi1 is expressed in vivo in intestinal stem cells. *Nat. Genet.* 40: 915–920.
 23. Montgomery, R. K., D. L. Carlone, C. A. Richmond, L. Farilla, M. E. G Kranendonk, D. E. Henderson, N. Yaa Baffour-Awuah, D. M. Ambruzs, L. K. Fogli, S. Algra, D. T. Breault, and by A. Robert Weinberg. Mouse telomerase reverse transcriptase (mTert) expression marks slowly cycling intestinal stem cells. .
 24. Powell, A. E., Y. Wang, Y. Li, E. J. Poulin, A. L. Means, M. K. Washington, J. N. Higginbotham, A. Juchheim, N. Prasad, S. E. Levy, Y. Guo, Y. Shyr, B. J. Aronow, K. M. Haigis, J. L. Franklin, and R. J. Coffey. 2012. The pan-ErbB negative regulator Lrig1 is an intestinal stem cell marker that functions as a tumor suppressor. *Cell* 149: 146–158.
 25. Ayyaz, A., S. Kumar, B. Sangiorgi, B. Ghoshal, J. Gosio, S. Ouladan, M. Fink, S. Barutcu, D. Trcka, J. Shen, K. Chan, J. L. Wrana, and A. Gregorieff. 2019. Single-cell transcriptomes of the regenerating intestine reveal a revival stem cell. *Nature* 569: 121–125.
 26. Zhu, G., J. Hu, and R. Xi. 2021. The cellular niche for intestinal stem cells: a team effort. *Cell Regen.* 10.
 27. Van Es, J. H., T. Sato, M. Van De Wetering, A. Lyubimova, A. Ng, Y. Nee, A. Gregorieff, N. Sasaki, L. Zeinstra, M. Van Den Born, J. Korving, A. C. M. Martens, N. Barker, A. Van Oudenaarden, and H. Clevers. 2012. Dll1 + secretory progenitor cells revert to stem cells upon crypt damage. .
 28. Tetteh, P. W., O. Basak, H. F. Farin, K. Wiebrands, K. Kretzschmar, H. Begthel, M. Van Den Born, J. Korving, F. De Sauvage, J. H. Van Es, A. Van Oudenaarden, and H. Clevers. 2016. Replacement of Lost Lgr5-Positive Stem Cells through Plasticity of Their Enterocyte-Lineage Daughters. *Cell Stem Cell* 18: 203–213.
 29. De Santa Barbara, P., G. R. Van Den Brink, and D. J. Roberts. 2003. Review Development and differentiation of the intestinal epithelium. *C. Cell. Mol. Life Sci* 60: 1322–1332.
 30. Snoeck, V., B. Goddeeris, and E. Cox. 2005. The role of enterocytes in the intestinal barrier function and antigen uptake. *Microbes Infect.* 7: 997–1004.
 31. Miron, N., and V. Cristea. 2011. Enterocytes: active cells in tolerance to food and microbial antigens in the gut. *ei_4523* 405..412. .
 32. Hooper, L. V. 2015. Epithelial Cell Contributions to Intestinal Immunity. *Adv. Immunol.* 126: 129–172.
 33. Macpherson, A. J., and T. Uhr. 2004. Induction of Protective IgA by Intestinal Dendritic Cells Carrying Commensal Bacteria. *Science (80-.)*. 303: 1662–1665.
 34. Kobayashi, N., D. Takahashi, S. Takano, S. Kimura, and K. Hase. 2019. The Roles of Peyer’s Patches and Microfold Cells in the Gut Immune System: Relevance to Autoimmune Diseases. *Front. Immunol.* 10: 2345.
 35. Dillon, A., and D. D. Lo. 2019. M cells: Intelligent engineering of mucosal immune surveillance. *Front. Immunol.* 10: 1499.

36. Cortez, V., and S. Schultz-Cherry. 2021. The role of goblet cells in viral pathogenesis. *FEBS J.* 288: 7060–7072.
37. Pelaseyed, T., J. H. Bergström, J. K. Gustafsson, A. Ermund, G. M. H. Birchenough, A. Schütte, S. van der Post, F. Svensson, A. M. Rodríguez-Piñero, E. E. L. Nyström, C. Wising, M. E. V. Johansson, and G. C. Hansson. 2014. The mucus and mucins of the goblet cells and enterocytes provide the first defense line of the gastrointestinal tract and interact with the immune system. *Immunol. Rev.* 260: 8–20.
38. Johansson, M. E. V, G. C. Hansson, M. E. V Johansson, H. Sjövall, and G. C. Hansson. 2013. The gastrointestinal mucus system in health and disease. *Nat. Publ. Gr.* 10: 352–361.
39. Peterson, L. W., and D. Artis. 2014. Intestinal epithelial cells: Regulators of barrier function and immune homeostasis. *Nat. Rev. Immunol.* 14: 141–153.
40. Gunawardene, A. R., B. M. Corfe, and C. A. Staton. 2011. Classification and functions of enteroendocrine cells of the lower gastrointestinal tract. *Int. J. Exp. Pathol.* 92: 219–231.
41. Ahlman, H., and O. Nilsson. 2001. The gut as the largest endocrine organ in the body. *Ann. Oncol.* 12: 63–68.
42. Guo, X., J. Lv, and R. Xi. 2021. The specification and function of enteroendocrine cells in *Drosophila* and mammals: a comparative review. *FEBS J.* 1–24.
43. Bevins, C. L., and N. H. Salzman. 2011. Paneth cells, antimicrobial peptides and maintenance of intestinal homeostasis. *Nat. Rev. Microbiol.* 9: 356–368.
44. Clevers, H. C., and C. L. Bevins. 2013. Paneth cells: Maestros of the small intestinal crypts. *Annu. Rev. Physiol.* 75: 289–311.
45. Meran, L., A. Baulies, and V. S. W. Li. 2017. Intestinal Stem Cell Niche: The Extracellular Matrix and Cellular Components. *Stem Cells Int.* 2017: 1–12.
46. Sasaki, N., N. Sachs, K. Wiebrands, S. I. J. Ellenbroek, A. Fumagalli, A. Lyubimova, H. Begthel, M. Den Van Born, J. H. Van Es, W. R. Karthaus, V. S. W. Li, C. López-Iglesias, P. J. Peters, J. Van Rheenen, A. Van Oudenaarden, and H. Clevers. 2016. Reg4⁺ deep crypt secretory cells function as epithelial niche for Lgr5⁺ stem cells in colon. *Proc. Natl. Acad. Sci. U. S. A.* 113: E5399–E5407.
47. Powell, D. W., I. V. Pinchuk, J. I. Saada, X. Chen, and R. C. Mifflin. 2011. Mesenchymal cells of the intestinal lamina propria. *Annu. Rev. Physiol.* 73: 213–237.
48. Strine, M. S., and C. B. Wilen. 2022. Tuft cells are key mediators of interkingdom interactions at mucosal barrier surfaces. *PLoS Pathog.* 18.
49. Harris, N. 2016. The enigmatic tuft cell in immunity: An intestinal cell stimulates the immune response to parasitic infections. *Science (80-)*. 351: 1264–1265.
50. Gerbe, F., E. Sidot, D. J. Smyth, M. Ohmoto, I. Matsumoto, V. Dardalhon, P. Cesses, L. Garnier, M. Pouzolles, B. Brulin, M. Bruschi, Y. H Marcus, V. S. Zimmermann, N. Taylor, R. M. Maizels, and P. Jay. 2016. Intestinal epithelial tuft cells initiate type 2 mucosal immunity to helminth parasites. *Nature* 529: 226–230.
51. Von Moltke, J., M. Ji, H.-E. Liang, and R. M. Locksley. 2016. Tuft-cell-derived IL-25 regulates an intestinal ILC2-epithelial response circuit. *Nature* 529.
52. Howitt, M. R., S. Lavoie, M. Michaud, A. M. Blum, S. V. Tran, J. V. Weinstock, C. A. Gallini, K. Redding, R. F. Margolskee, L. C. Osborne, D. Artis, and W. S. Garrett. 2016. Tuft cells, taste-chemosensory cells, orchestrate

- parasite type 2 immunity in the gut. *Science* 351: 1329–1333.
53. Schneider, C., C. E. O’Leary, and R. M. Locksley. 2019. Regulation of immune responses by tuft cells. *Nat. Rev. Immunol.* 2019 19: 584–593.
54. Perochon, J., L. R. Carroll, and J. B. Cordero. 2018. Wnt signalling in intestinal stem cells: Lessons from mice and flies. *Genes (Basel)*. 9.
55. Biswas, S., H. Davis, S. Irshad, T. Sandberg, D. Worthley, and S. Leedham. 2015. Microenvironmental control of stem cell fate in intestinal homeostasis and disease. *J. Pathol. J Pathol* 237: 135–145.
56. Mah, A. T., K. S. Yan, and C. J. Kuo. 2016. The Journal of Physiology Wnt pathway regulation of intestinal stem cells. *Authors. J. Physiol. C* 594: 4837–4847.
57. Czerwinski, M., N. F. Shroyer, and J. R. Spence. 2018. WNT Signaling in the Intestine: Development, Homeostasis, Disease. *Physiol. Gastrointest. Tract Sixth Ed.* 1–2: 185–196.
58. Korinek, V., N. Barker, P. Moerer, E. Van Donselaar, G. Huls, P. J. Peters, and H. Clevers. 1998. Depletion of epithelial stem-cell compartments in the small intestine of mice lacking Tcf-4. *Nat. Genet.* 19: 379–383.
59. Fevr, T., S. Robine, D. Louvard, and J. Huelsken. 2007. Wnt/ β -Catenin Is Essential for Intestinal Homeostasis and Maintenance of Intestinal Stem Cells. *Mol. Cell. Biol.* 27: 7551–7559.
60. Krausova, M., and V. Korinek. 2014. Wnt signaling in adult intestinal stem cells and cancer. *Cell. Signal.* 26: 570–579.
61. Kosinski, C., V. S. W Li, A. S. Y Chan, J. Zhang, C. Ho, W. Yin Tsui, T. Leung Chan, R. C. Mifflin, D. W. Powell, S. Tsan Yuen, S. Yi Leung, and X. Chen. 2007. *Gene expression patterns of human colon tops and basal crypts and BMP antagonists as intestinal stem cell niche factors.*,
62. Wang, S., and Y. G. Chen. 2018. BMP signaling in homeostasis, transformation and inflammatory response of intestinal epithelium. *Sci. China. Life Sci.* 61: 800–807.
63. Haramis, A. P. G., H. Begthel, M. Van Den Born, J. Van Es, S. Jonkheer, G. J. A. Offerhaus, and H. Clevers. 2004. De novo crypt formation and juvenile polyposis on BMP inhibition in mouse intestine. *Science* 303: 1684–1686.
64. Qi, Z., Y. Li, B. Zhao, C. Xu, Y. Liu, H. Li, B. Zhang, X. Wang, X. Yang, W. Xie, B. Li, J. D. J. Han, and Y. G. Chen. 2017. BMP restricts stemness of intestinal Lgr5⁺ stem cells by directly suppressing their signature genes. *Nat. Commun.* 2017 8: 1–14.
65. Auclair, B. A., Y. D. Benoit, N. Rivard, Y. Mishina, and N. Perreault. 2007. Bone Morphogenetic Protein Signaling Is Essential for Terminal Differentiation of the Intestinal Secretory Cell Lineage. *Gastroenterology* 133: 887–896.
66. Zhang, Y., and J. Que. 2020. BMP Signaling in Development, Stem Cells, and Diseases of the Gastrointestinal Tract. *Annu. Rev. Physiol.* 82: 251–273.
67. Büller, N. V. J. A., S. L. Rosekrans, J. Westerlund, and G. R. van den Brink. 2012. Hedgehog signaling and maintenance of homeostasis in the intestinal epithelium. *Physiology* 27: 148–155.
68. Van Den Brink, G. R. 2007. Hedgehog signaling in development and homeostasis of the gastrointestinal tract. *Physiol. Rev.* 87: 1343–1375.

69. Kolterud, Å., A. S. Grosse, W. J. Zacharias, K. D. Walton, K. E. Kretovich, B. B. Madison, M. Waghray, J. E. Ferris, C. Hu, J. L. Merchant, A. A. Dlugosz, A. H. Kottmann, and D. L. Gumucio. 2009. Paracrine Hedgehog Signaling in Stomach and Intestine: New Roles for Hedgehog in Gastrointestinal Patterning. *Gastroenterology* 137: 618–628.
70. van Dop, W. A., A. Uhmman, M. Wijgerde, E. Sleddens-Linkels, J. Heijmans, G. J. Offerhaus, M. A. van den Bergh Weerman, G. E. Boeckstaens, D. W. Hommes, J. C. Hardwick, H. Hahn, and G. R. van den Brink. 2009. Depletion of the Colonic Epithelial Precursor Cell Compartment Upon Conditional Activation of the Hedgehog Pathway. *Gastroenterology* 136: 2195-2203.e7.
71. Van Dop, W. A., J. Heijmans, N. V. J. A. Büller, S. A. Snoek, S. L. Rosekrans, E. A. Wassenberg, M. A. Van Den Bergh Weerman, B. Lanske, A. R. Clarke, D. J. Winton, M. Wijgerde, G. J. Offerhaus, D. W. Hommes, J. C. Hardwick, W. J. De Jonge, I. Biemond, and G. R. Van Den Brink. 2010. Loss of Indian Hedgehog Activates Multiple Aspects of a Wound Healing Response in the Mouse Intestine. *Gastroenterology* 139: 1665-1676.e10.
72. Kosinski, C., D. E. Stange, C. Xu, A. S. Chan, C. Ho, S. T. Yuen, R. C. Mifflin, D. W. Powell, H. Clevers, S. Y. Leung, and X. Chen. 2010. Indian hedgehog regulates intestinal stem cell fate through epithelial-mesenchymal interactions during development. *Gastroenterology* 139: 893–903.
73. Liang, S., X. Li, and X. Wang. 2019. Notch Signaling in Mammalian Intestinal Stem Cells: Determining Cell Fate and Maintaining Homeostasis. *Curr. Stem Cell Res. Ther.* 14: 583–590.
74. Sancho, R., C. A. Cremona, and A. Behrens. 2015. Stem cell and progenitor fate in the mammalian intestine: Notch and lateral inhibition in homeostasis and disease. *EMBO Rep.* 16: 571–581.
75. Fre, S., M. Huyghe, P. Mourikis, S. Robine, D. Louvard, and S. Artavanis-Tsakonas. 2005. Notch signals control the fate of immature progenitor cells in the intestine. *Nature* 435: 964–968.
76. Kim, T. H., S. Escudero, and R. A. Shivdasani. 2012. Intact function of Lgr5 receptor-expressing intestinal stem cells in the absence of Paneth cells. *Proc. Natl. Acad. Sci. U. S. A.* 109: 3932–3937.
77. Owens, B. M. J., and A. Simmons. 2012. Intestinal stromal cells in mucosal immunity and homeostasis. *Mucosal Immunol.* 2013 62 6: 224–234.
78. McCarthy, N., E. Manieri, E. E. Storm, A. Saadatpour, A. M. Luoma, V. N. Kapoor, S. Madha, L. T. Gaynor, C. Cox, S. Keerthivasan, K. Wucherpfennig, G. C. Yuan, F. J. de Sauvage, S. J. Turley, and R. A. Shivdasani. 2020. Distinct Mesenchymal Cell Populations Generate the Essential Intestinal BMP Signaling Gradient. *Cell Stem Cell* 26: 391.
79. Mifflin, R. C., I. V Pinchuk, J. I. Saada, and D. W. Powell. 2011. Intestinal myofibroblasts: targets for stem cell therapy. *Am J Physiol Gastrointest Liver Physiol* 300: 684–696.
80. Kinchen, J., H. H. Chen, K. Parikh, A. Antanaviciute, M. Jagielowicz, D. Fawcner-Corbett, N. Ashley, L. Cubitt, E. Mellado-Gomez, M. Attar, E. Sharma, Q. Wills, R. Bowden, F. C. Richter, D. Ahern, K. D. Puri, J. Henault, F. Gervais, H. Koohy, and A. Simmons. 2018. Structural Remodeling of the Human Colonic Mesenchyme in Inflammatory Bowel Disease. *Cell* 175: 372-386.e17.
81. Aoki, R., M. Shoshkes-Carmel, N. Gao, S. Shin, C. L. May, M. L. Golson, A. M. Zahm, M. Ray, C. L. Wiser, C. V. E. Wright, and K. H. Kaestner. 2016. Foxl1-Expressing Mesenchymal Cells Constitute the Intestinal Stem Cell

Niche. *CMGH* 2: 175–188.

82. Kim, J. E., L. Fei, W. C. Yin, S. Coquenlorge, A. Rao-Bhatia, X. Zhang, S. S. W. Shi, J. H. Lee, N. A. Hahn, W. Rizvi, K. H. Kim, H. K. Sung, C. chung Hui, G. Guo, and T. H. Kim. 2020. Single cell and genetic analyses reveal conserved populations and signaling mechanisms of gastrointestinal stromal niches. *Nat. Commun.* 11.

83. McAnulty, R. J. 2007. Fibroblasts and myofibroblasts: Their source, function and role in disease. *Int. J. Biochem. Cell Biol.* 39: 666–671.

84. Havran, W. L., J. M. Jameson, and D. A. Witherden. 2005. Epithelial Cells and Their Neighbors. III. Interactions between intraepithelial lymphocytes and neighboring epithelial cells. *Am J Physiol Gastrointest Liver Physiol* 289: 627–630.

85. Pinchuk, I. V., R. C. Mifflin, J. I. Saada, and D. W. Powell. 2010. Intestinal mesenchymal cells. *Curr. Gastroenterol. Rep.* 12: 310–318.

86. Lei, N. Y., Z. Jabaji, J. Wang, V. S. Joshi, and G. J. Brinkley. 2014. Intestinal Subepithelial Myofibroblasts Support the Growth of Intestinal Epithelial Stem Cells. *PLoS One* 9: 84651.

87. San Roman, A. K., C. D. Jayewickreme, L. C. Murtaugh, and R. A. Shivdasani. 2014. Wnt secretion from epithelial cells and subepithelial myofibroblasts is not required in the mouse intestinal stem cell niche in vivo. *Stem Cell Reports* 2: 127–134.

88. Popescu, L. M., and M. S. Faussone-Pellegrini. 2010. TELOCYTES - a case of serendipity: The winding way from Interstitial Cells of Cajal (ICC), via Interstitial Cajal-Like Cells (ICLC) to TELOCYTES. *J. Cell. Mol. Med.* 14: 729–740.

89. McCarthy, N., J. Kraiczy, and R. A. Shivdasani. 2020. Cellular and molecular architecture of the intestinal stem cell niche. *Nat. Cell Biol.* 22: 1033–1041.

90. Kaestner, K. H. 2019. The Intestinal Stem Cell Niche: A Central Role for Foxl1-Expressing Subepithelial Telocytes. *Cmgh* 8: 111–117.

91. Shoshkes-Carmel, M., Y. J. Wang, K. J. Wangenstein, B. Tóth, A. Kondo, E. E. Massassa, S. Itzkovitz, and K. H. Kaestner. 2018. Subepithelial telocytes are an important source of Wnts that supports intestinal crypts. *Nat.* 2018 5577704 557: 242–246.

92. Vannucchi, M. G., C. Traini, M. Manetti, L. Ibba-Manneschi, and M. S. Faussone-Pellegrini. 2013. Telocytes express PDGFR α in the human gastrointestinal tract. *J. Cell. Mol. Med.* 17: 1099–1108.

93. Degirmenci, B., T. Valenta, S. Dimitrieva, G. Hausmann, and K. Basler. 2018. GLI1-expressing mesenchymal cells form the essential Wnt-secreting niche for colon stem cells. *Nature* 558: 449–453.

94. David, M. B., T. Valenta, H. Fazilaty, G. Hausmann, and K. Basler. 2020. Distinct populations of crypt-associated fibroblasts act as signaling hubs to control colon homeostasis. *PLoS Biol.* 18.

95. Stzepourginski, I., G. Nigro, J. M. Jacob, S. Dulauroy, P. J. Sansonetti, G. Eberl, and L. Peduto. 2017. CD34+ mesenchymal cells are a major component of the intestinal stem cells niche at homeostasis and after injury. *Proc. Natl. Acad. Sci. U. S. A.* 114: E506–E513.

96. Xavier, R. J., and D. K. Podolsky. 2007. Unravelling the pathogenesis of inflammatory bowel disease. *Nature* 448: 427–434.

97. Boirivant, M., and A. Cossu. 2012. Inflammatory bowel disease. *Oral Dis.* 18: 1–15.
98. Kaistha, A., and J. Levine. 2014. Inflammatory Bowel Disease: The Classic Gastrointestinal Autoimmune Disease. *Curr. Probl. Pediatr. Adolesc. Health Care* 44: 328–334.
99. Baumgart, D. C., and W. J. Sandborn. 2012. Crohn’s disease. *Lancet* 380: 1590–1605.
100. Hollander, D. 2009. The Intestinal Permeability Barrier: A Hypothesis as to Its Regulation and Involvement in Crohn’s Disease. <https://doi.org/10.3109/00365529209011172> 27: 721–726.
101. Turpin, W., S. H. Lee, J. A. Raygoza Garay, K. L. Madsen, J. B. Meddings, L. Bedrani, N. Power, O. Espin-Garcia, W. Xu, M. I. Smith, A. M. Griffiths, P. Moayyedi, D. Turner, E. G. Seidman, A. H. Steinhart, J. K. Marshall, K. Jacobson, D. Mack, H. Huynh, C. N. Bernstein, A. D. Paterson, M. Abreu, P. Beck, K. Croitoru, L. Dieleman, B. Feagan, A. Griffiths, D. Guttman, G. Kaplan, D. O. Krause, K. Madsen, J. Marshall, M. Ropeleski, E. Seidman, M. Silverberg, S. Snapper, A. Stadnyk, H. Steinhart, M. Surette, T. Walters, B. Vallance, G. Aumais, A. Bitton, M. Cino, J. Critch, L. Denson, C. Deslandres, W. El-Matary, H. Herfarth, P. Higgins, J. Hyams, J. McGrath, A. Otley, R. Panacionne, R. Baldassano, C. Hedin, S. Hussey, H. Hyams, D. Keljo, D. Kevans, C. Lees, S. Murthy, R. Panaccione, N. Parekh, S. Plamondon, G. Radford-Smith, J. Rosh, D. Rubin, M. Schultz, and C. Siegel. 2020. Increased Intestinal Permeability Is Associated With Later Development of Crohn’s Disease. *Gastroenterology* 159: 2092-2100.e5.
102. Munkholm, P., E. Langholz, D. Hollander, K. Thornberg, M. Orholm, K. D. Katz, and V. Binder. 1994. Intestinal permeability in patients with Crohn’s disease and ulcerative colitis and their first degree relatives. *Gut* 35: 68–72.
103. Smillie, C. S., M. Biton, J. Ordovas-Montanes, K. M. Sullivan, G. Burgin, D. B. Graham, R. H. Herbst, N. Rogel, M. Slyper, J. Waldman, M. Sud, E. Andrews, G. Velonias, A. L. Haber, K. Jagadeesh, S. Vickovic, J. Yao, C. Stevens, D. Dionne, L. T. Nguyen, A. C. Villani, M. Hofree, E. A. Creasey, H. Huang, O. Rozenblatt-Rosen, J. J. Garber, H. Khalili, A. N. Desch, M. J. Daly, A. N. Ananthakrishnan, A. K. Shalek, R. J. Xavier, and A. Regev. 2019. Intra- and Inter-cellular Rewiring of the Human Colon during Ulcerative Colitis. *Cell* 178: 714-730.e22.
104. Nataro, J. P., and J. B. Kaper. 1998. *Diarrheagenic Escherichia coli*. American Society for Microbiology.
105. Deborah Chen, H., and G. Frankel. 2005. Enteropathogenic Escherichia coli: Unravelling pathogenesis. *FEMS Microbiol. Rev.* 29: 83–98.
106. Kaper, J. B., J. P. Nataro, and H. L. T. Mobley. 2004. Pathogenic Escherichia coli. *Nat. Rev. Microbiol.* 2: 123–140.
107. Bardiau, M., M. Szalo, and J. G. Mainil. 2010. Initial adherence of EPEC, EHEC and VTEC to host cells. *Vet. Res.* 41.
108. Croxen, M. A., R. J. Law, R. Scholz, K. M. Keeney, M. Wlodarska, and B. B. Finlay. 2013. Recent advances in understanding enteric pathogenic Escherichia coli. *Clin. Microbiol. Rev.* 26: 822–880.
109. Collins, J. W., K. M. Keeney, V. F. Crepin, V. A. K. Rathinam, K. A. Fitzgerald, B. B. Finlay, and G. Frankel. 2014. Citrobacter rodentium: infection, inflammation and the microbiota. *Nat. Rev. Microbiol.* 2014 129 12: 612–623.
110. Koroleva, E. P., S. Halperin, E. O. Gubernatorova, E. Macho-Fernandez, C. M. Spencer, and A. V. Tumanov.

2015. *Citrobacter rodentium*-induced colitis: A robust model to study mucosal immune responses in the gut. *J. Immunol. Methods* 421: 61–72.
111. Vallance, B. A., W. Deng, K. Jacobson, and B. B. Finlay. 2003. Host susceptibility to the attaching and effacing bacterial pathogen *Citrobacter rodentium*. *Infect. Immun.* 71: 3443–3453.
112. Borenshtein, D., P. R. Nambiar, E. B. Groff, J. G. Fox, and D. B. Schauer. 2007. Development of fatal colitis in FVB Mice infected with *Citrobacter rodentium*. *Infect. Immun.* 75: 3271–3281.
113. Papapietro, O., S. Teatero, A. Thanabalasuriar, K. E. Yuki, E. Diez, L. Zhu, E. Kang, S. Dhillon, A. M. Muise, Y. Durocher, M. M. Marcinkiewicz, D. Malo, and S. Gruenheid. 2013. ARTICLE R-Spondin 2 signalling mediates susceptibility to fatal infectious diarrhoea. *Nat. Commun.* .
114. Jin, Y. R., and J. K. Yoon. 2012. The R-spondin family of proteins: Emerging regulators of WNT signaling. *Int. J. Biochem. Cell Biol.* 44: 2278–2287.
115. Kang, E., M. Yousefi, and S. Gruenheid. 2016. R-Spondins Are Expressed by the Intestinal Stroma and are Differentially Regulated during *Citrobacter rodentium*-and DSS-Induced Colitis in Mice. .
116. Stuart, T., A. Butler, P. Hoffman, C. Hafemeister, E. Papalexi, W. M. Mauck, Y. Hao, M. Stoeckius, P. Smibert, and R. Satija. 2019. Comprehensive Integration of Single-Cell Data. *Cell* 177: 1888-1902.e21.
117. Zhang, H., G. Carnevale, B. Polese, M. Simard, B. Thurairajah, N. Khan, M. E. Gentile, G. Fontes, D. C. Vinh, R. Pouliot, and I. L. King. 2019. CD109 Restrains Activation of Cutaneous IL-17-Producing $\gamma\delta$ T Cells by Commensal Microbiota. *Cell Rep.* 29: 391-405.e5.
118. Mii, S., A. Enomoto, Y. Shiraki, T. Taki, Y. Murakumo, and M. Takahashi. 2019. CD109: a multifunctional GPI-anchored protein with key roles in tumor progression and physiological homeostasis. *Pathol. Int.* 69: 249–259.
119. Clevers, H. 2016. Modeling Development and Disease with Organoids. *Cell* 165: 1586–1597.
120. Sprangers, J., I. C. Zaalberg, and M. M. Maurice. 2021. Organoid-based modeling of intestinal development, regeneration, and repair. *Cell Death Differ.* 28: 95–107.
121. Fordham, R. P., S. Yui, N. R. F. Hannan, C. Soendergaard, A. Madgwick, P. J. Schweiger, O. H. Nielsen, L. Vallier, R. A. Pedersen, T. Nakamura, M. Watanabe, and K. B. Jensen. 2013. Transplantation of expanded fetal intestinal progenitors contributes to colon regeneration after injury. *Cell Stem Cell* 13: 734–744.
122. Fawcner-Corbett, D., A. S. Gerós, A. Antanaviciute, and A. Simmons. 2021. Isolation of human fetal intestinal cells for single-cell RNA sequencing. *STAR Protoc.* 2: 100890.
123. Roulis, M., A. Kaklamanos, M. Scherthanner, P. Bielecki, J. Zhao, E. Kaffe, L.-S. Frommelt, R. Qu, M. S. Knapp, A. Henriques, N. Chalkidi, V. Koliaraki, J. Jiao, J. R. Brewer, M. Bacher, H. N. Blackburn, X. Zhao, R. M. Breyer, V. Aidinis, D. Jain, B. Su, H. R. Herschman, Y. Kluger, G. Kollias, and R. A. Flavell. 2020. Paracrine orchestration of intestinal tumorigenesis by a mesenchymal niche. *Nature* 580: 524–529.
124. Smith, W. L., Y. Urade, and P. J. Jakobsson. 2011. Enzymes of the Cyclooxygenase Pathways of Prostanoid Biosynthesis. *Chem. Rev.* 111: 5821.
125. Kalinski, P. 2022. 2 Prostaglandin E Regulation of Immune Responses by. *J Immunol Ref.* 188: 21–28.
126. Silberger, D. J., C. L. Zindl, and C. T. Weaver. 2017. *Citrobacter rodentium*: A model enteropathogen for understanding the interplay of innate and adaptive components of type 3 immunity. *Mucosal Immunol.* 10: 1108–

1117.

127. Grauel, A. L., B. Nguyen, D. Ruddy, T. Laszewski, S. Schwartz, J. Chang, J. Chen, M. Piquet, M. Pelletier, Z. Yan, N. D. Kirkpatrick, J. Wu, A. deWeck, M. Riester, M. Hims, F. C. Geyer, J. Wagner, K. MacIsaac, J. Deeds, R. Diwanji, P. Jayaraman, Y. Yu, Q. Simmons, S. Weng, A. Raza, B. Minie, M. Dostalek, P. Chikkegowda, V. Ruda, O. Iartchouk, N. Chen, R. Thierry, J. Zhou, I. Pruteanu-Malinici, C. Fabre, J. A. Engelman, G. Dranoff, and V. Cremasco. 2020. TGF β -blockade uncovers stromal plasticity in tumors by revealing the existence of a subset of interferon-licensed fibroblasts. *Nat. Commun.* 2020 11: 1–17.
128. Zhang, Y. G., M. Singhal, Z. Lin, C. Manzella, A. Kumar, W. A. Alrefai, P. K. Dudeja, S. Saksena, J. Sun, and R. K. Gill. 2018. Infection with enteric pathogens *Salmonella typhimurium* and *Citrobacter rodentium* modulate TGF- β /Smad signaling pathways in the intestine. *Gut Microbes* 9: 326–337.
129. Saada, J. I., I. V. Pinchuk, C. A. Barrera, P. A. Adegboyega, G. Suarez, R. C. Mifflin, J. F. Di Mari, V. E. Reyes, and D. W. Powell. 2006. Subepithelial Myofibroblasts are Novel Nonprofessional APCs in the Human Colonic Mucosa. *J. Immunol.* 177: 5968–5979.
130. Ouladan, S., A. Gregorieff, M.-I. Garcia, and N. Soshnikova. 2021. Taking a Step Back: Insights into the Mechanisms Regulating Gut Epithelial Dedifferentiation. *Int. J. Mol. Sci.* 2021, Vol. 22, Page 7043 22: 7043.
131. Yui, S., L. Azzolin, M. Maimets, M. T. Pedersen, R. P. Fordham, S. L. Hansen, H. L. Larsen, J. Guiu, M. R. P. Alves, C. F. Rundsten, J. V. Johansen, Y. Li, C. D. Madsen, T. Nakamura, M. Watanabe, O. H. Nielsen, P. J. Schweiger, S. Piccolo, and K. B. Jensen. 2018. YAP/TAZ-Dependent Reprogramming of Colonic Epithelium Links ECM Remodeling to Tissue Regeneration. *Cell Stem Cell* 22: 35.
132. Miyoshi, H., K. L. VanDussen, N. P. Malvin, S. H. Ryu, Y. Wang, N. M. Sonnek, C. Lai, and T. S. Stappenbeck. 2017. Prostaglandin E2 promotes intestinal repair through an adaptive cellular response of the epithelium. *EMBO J.* 36: 5.